Reactivity and Dynamics of H2S, NO, and O-2 Interacting with Hemoglobins from Lucina pectinata

7 AUTHORS, INCLUDING:

Byung-Kuk Yoo
California Institute of Technology

24 PUBLICATIONS **126** CITATIONS

SEE PROFILE

Ruth Pietri
University of Puerto Rico at Cayey

23 PUBLICATIONS **267** CITATIONS

SEE PROFILE

Isabelle Lamarre
École Polytechnique

26 PUBLICATIONS **531** CITATIONS

SEE PROFILE

Juan López-Garriga
University of Puerto Rico at Mayagüez

63 PUBLICATIONS **818** CITATIONS

SEE PROFILE

# Reactivity and Dynamics of H$_2$S, NO, and O$_2$ Interacting with Hemoglobins from *Lucina pectinata*

Cacimar Ramos-Alvarez,[†] Byung-Kuk Yoo,[‡,§] Ruth Pietri,[†] Isabelle Lamarre,[‡] Jean-Louis Martin,[‡] Juan Lopez-Garriga,[†] and Michel Negrerie*[,‡]

[†]Department of Chemistry, University of Puerto Rico, Mayagüez Campus, Mayagüez 00680, Puerto Rico
[‡]Laboratoire d'Optique et Biosciences, INSERM, Ecole Polytechnique, 91128 Palaiseau, France

S Supporting Information

ABSTRACT: Hemoglobin HbI from the clam *Lucina pectinata* is involved in H$_2$S transport, whereas homologous heme protein HbII/III is involved in O$_2$ metabolism. Despite similar tertiary structures, HbI and HbII/III exhibit very different reactivity toward heme ligands H$_2$S, O$_2$, and NO. To investigate this reactivity at the heme level, we measured the dynamics of ligand interaction by time-resolved absorption spectroscopy in the picosecond to nanosecond time range. We demonstrated that H$_2$S can be photodissociated from both ferric and ferrous HbI. H$_2$S geminately rebinds to ferric and ferrous out-of-plane iron with time constants (τ_{gem}) of 12 and 165 ps, respectively, with very different proportions of photodissociated H$_2$S exiting the protein (24% in ferric and 80% in ferrous HbI). The Gln(E7)His mutation considerably changes H$_2$S dynamics in ferric HbI, indicating the role of Gln(E7) in controling H$_2$S reactivity. In ferric HbI, the rate of diffusion of H$_2$S from the solvent into the heme pocket (k_{entry}) is 0.30 μM^{-1} s^{-1}. For the HbII/III−O$_2$ complex, we observed mainly a six-coordinate vibrationally excited heme−O$_2$ complex with O$_2$ still bound to the iron. This explains the low yield of O$_2$ photodissociation and low k_{off} from HbII/III, compared with those of HbI and Mb. Both isoforms behave very differently with regard to NO and O$_2$ dynamics. Whereas the amplitude of geminate rebinding of O$_2$ to HbI (38.5%) is similar to that of myoglobin (34.5%) in spite of different distal heme sites, it appears to be much larger for HbII/III (77%). The distal Tyr(B10) side chain present in HbII/III increases the energy barrier for ligand escape and participates in the stabilization of bound O$_2$ and NO.
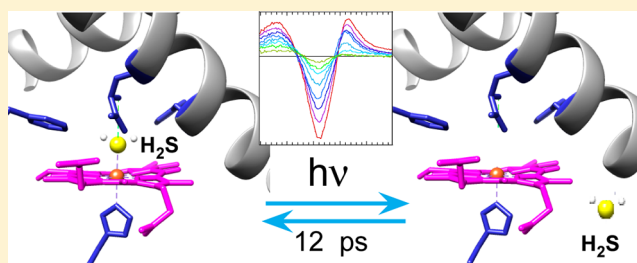
In shallow sea waters of mangrove swamps whose sediments contain sulfide, the mollusc *Lucina pectinata* lives with symbiont bacteria, which utilize the reductant H$_2$S.[1] This clam has developed various heme proteins in the gill cells called hemoglobin[2] after the mammalian O$_2$ carrier, which has the same tertiary structure. Monomeric hemoglobin isoform HbI is involved in H$_2$S transport because of its much higher affinity for H$_2$S in the ferric state compared to other heme proteins.[2] The other tetramer isoforms HbII/III from the same clam share 75% homologous sequences[2] and are involved in O$_2$ metabolism, like the mammalian Hb counterpart. Isolated HbII and HbIII form dimers, whereas a mixture of HbII/III yields tetramers. These three Hbs have the same tertiary fold as myoglobin[3] (Figure 1), yet HbI and HbII/III exhibit different reactivity toward small heme ligands (H$_2$S, O$_2$, and NO). The very broad range of heme ligand affinity and redox reactivity in the globin family is tightly governed by diverse combinations of side-chain substitutions within the heme cavity and was subject to numerous mutational studies of the dynamics and binding of CO,[4,5] NO,[6,7] O$_2$,[8,9] and H$_2$S[10] to globins from various species.

The interaction between H$_2$S and proteins is not limited to molluscs. As a recently recognized messenger in vertebrates[11] with an unknown specific receptor, H$_2$S is the subject of a growing number of studies.[12−14] Although sulfhydration of target side chains seems to be the principal mode of action of H$_2$S, it may bind to particular hemeproteins[14] such as neuroglobin[15] and cytochrome oxidase.[16] Furthermore, the enzyme that produces H$_2$S, human cystathionine β-synthase, possesses itself a heme cofactor whose function is not yet known with certainty[17] but may have a regulatory role.[18] In addition, several studies have pointed out the coupling between the signaling pathways involving H$_2$S, CO, and NO.[19−22] For these reasons, there necessarily exists discrimination among heme ligands H$_2$S, O$_2$, and NO, both for the regulation of H$_2$S signaling in vertebrates and for the functioning of mollusc hemoglobins in metabolism. The physiologically relevant redox state of HbI is ferric for binding H$_2$S with an affinity for this ligand much higher than for ferric HbI ($K_D \sim 1$ nM) or for the other ferric isoform HbII/III ($K_D \sim 15$ μM).[2] Ferrous HbI and HbII/III have very similar dissociation constants for O$_2$ ($K_D = 0.4$ and 0.3 μM, respectively), but in contrast, these K_D values result from very different kinetic constants that are much slower

A

```
Hb I    ~~SLEAAQKSNVTSSWAKASAAWGTAGPEFF MALFDAHDD  38
Mb      ~~GLSDGEWQQVLNVWGKVEADIAGHGQEVL IRLFTGHPE   38
Hb II   ~TTLTNPQKAAIRSSWSKFMDNGVSNGGQFY MDLFKAHPE   39
Hb III  SSGLTGPQKAALKSSWSRFMDNAVTNGTNFY MDLFKAYPD   40

Hb I    VFAKFSGLFSG~~AAKG~~T~VKNTPEMAAQ AQSFKGLVS    73
Mb      TLEKFD~KF~K~~HLKTEAE~MKASEDLKKH GTVVLTALG    73
Hb II   TLTPFKSLFG~GLTL~~~~AQLQDNPKMKAQ SLVFCNGMS    74
Hb III  TLTPFKSLFE~~~~~DVSFNQMTDHPTMKAQ ALVFCDFMS    75

Hb I    NWVDNLDNAGALEGQCKTFAANHK~ARGISAGQLEAAFKV     112
Mb      GILKKK~GH~~HEAELKPLAQSHATKHKIPIKYLEFISDA     110
Hb II   SFVDHLDDNDMLVVLIQKMAKLHN~NRGIRASDLRTAYDI     113
Hb III  SFVDNLDDHEVLVVLLQKMAKLH~FNRGIRIKELRDGYGV     114

Hb I    LSGFMK~S~Y~~~GG~~~DEGAWTAVAGALMGEIEPDM~~     142
Mb      IIHVLHSKH~PGDF~GADAQGAMTKALELFRNDIAAKYKE     148
Hb II   LIHYMEDHNH~~~MVG~GAKDAWEVFVGFICKTLGDYMKE     149
Hb III  LLRYLEDHCH~~~~VEGSTKNAWEDFIAYICRVQGDFMKE     150

Hb I    ~~~~~  142
Mb      LGFQG  153
Hb II   LS~~~  151
Hb III  RL~~~  152
```
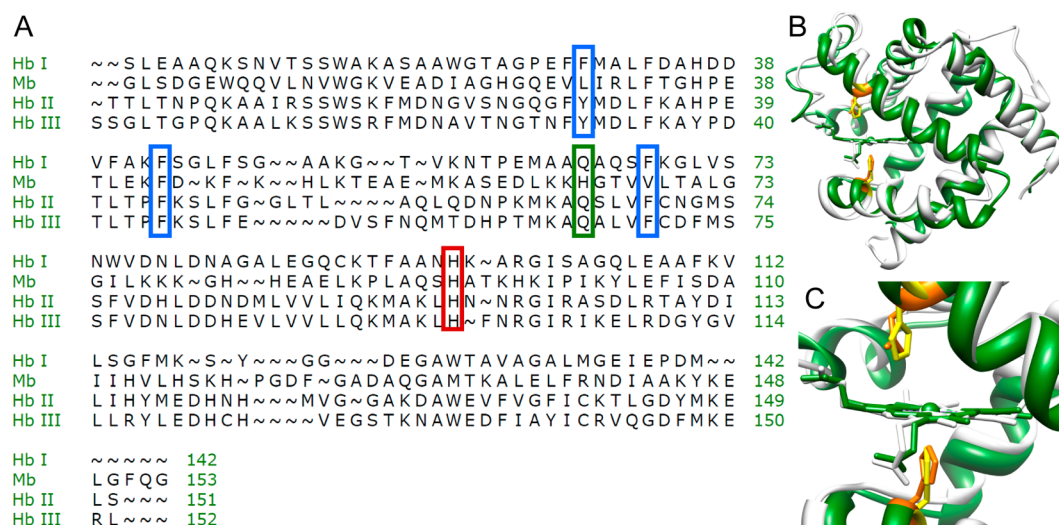
B

C

Figure 1. (A) Multiple-sequence alignment of the three types of hemoglobin from *L. pectinata* compared with horse heart myoglobin. The proximal His96 is boxed in red; homologous distal Phe/Tyr(B10), Phe(CD1), and Phe(E11) are boxed in blue, and Gln(E7) is boxed in green. (B) Superposition of structures of HbI [Protein Data Bank (PDB) entry 1FLP] and Mb (PDB entry 1YMB) conducted using Chimera. (C) Close-up view of the heme pocket. The proximal His97 and distal Gln64 in the heme pocket of HbI are colored orange, whereas His93 and His64 in Mb in the heme pocket are colored yellow.

for HbII/III by a factor of 440 for k_{on} and 610 for k_{off} than for HbI. Consequently, ligand discrimination implies equilibrium affinity differences and can be explained not only by ligand reactivity at the iron level but also by different energy barriers for ligand dynamics from the solvent to the heme pocket and reverse pathway.

To investigate the interaction of the three heme ligands, H_2S, O_2, and NO, with the Hb isoforms from *L. pectinata*, we measured the ligand dynamics within the Hb heme pocket in the picosecond to nanosecond time range by time-resolved absorption spectroscopy. This methodology allowed us to correlate ligand dynamics with the reactivity of heme proteins. The photodissociation of a ligand from the heme with a 50 fs laser pulse allowed us to create a synchronized population of protein−ligand pairs whose dissociated ligand starts its dynamics from the distal heme pocket and whose evolution of the heme state is transiently probed. Here, we report the parameters of ligand dynamics (H_2S, O_2, and NO) revealing the energy barriers, correlated with the association and dissociation rates, which are tuned by protein sequence and folding.

■ MATERIALS AND METHODS

We have studied the native monomer HbI, the native tetramer HbII/HbIII purified from the tissue, and the recombinant WT HbI protein, which has exactly the same properties as the native form. We have also expressed two mutants of HbI whose Gln(E7) is involved in the hydrogen bond network within the distal heme pocket.

Purification of Native Samples. *L. pectinata* clams were collected from the southwest mangrove swaps of Puerto Rico. The extraction, isolation, and purification of hemoglobins were conducted following the method described previously[23] with some modifications. Briefly, the gills were dissected from the clams and homogenized in a pH 7.5 phosphate buffer solution. This solution was centrifuged at 3000 rpm for 30 min, and the supernatant was collected, yielding the raw extract, a mixture of hemoglobins and proteins from the gill. Separation of HbI and HbII/HbIII from the raw extract was conducted in a Hi-Load 26/60 Superdex 200 gel filtration column using the

AKTA fast protein liquid chromatography (FPLC) system (Amersham Bioscience). The eluted colored fractions that correspond to HbI and HbII/III were concentrated using a Millipore ultrafiltration system. The purity of each protein was confirmed by the presence of a single band in a sodium dodecyl sulfate−polyacrylamide gel electrophoresis (SDS−PAGE) gel.

Protein Expression and Purification. Recombinant HbI and HbI mutants were obtained following the previously published protocol.[23,24] Briefly, the HbI coding region was obtained by reverse transcription polymerase chain reaction amplification from the total *L. pectinata* gill RNA and cloned into the pET28(a+) vector. The wild-type recombinant protein was expressed in *Escherichia coli* Bli5 cells transformed with the desired constructs containing a polyhistidine tag. Two days prior to the large scale fermentation, an overnight culture from a frozen stock (1 mL) was grown in 50 mL of Terrific Broth EZ mix medium containing kanamycin and chloramphenicol antibiotics. After 12 h, an aliquot of 1 mL was extracted and regrown in 50 mL of fresh medium in a water bath shaker at 37 °C. This overnight 50 mL cell culture was used to inoculate 500 mL of fresh TB medium containing the two antibiotics. After a 12 h incubation, the 500 mL culture was used to inoculate a 5 L fermentor (New Brunswick Bioflow). The fermentor medium was prepared by adding 54 g of tryptone, 108 g of yeast extract, and 36 mL of glycerol to 4.5 L of distilled water. The sealed bioreactor was sterilized and equilibrated at 37 °C, and the medium was inoculated with 500 mL of the previous culture and induced with 1 mM IPTG, 1% glucose, and 30 μg/mL hemin chloride. After 12 h, the cells were harvested by centrifugation of the medium broth, and the pellets were stored at −80 °C for further lysis and purification.

The stored pellets were lysed with lysozyme and protease inhibitor for 30 min in an ice bath and centrifuged (3500 rpm) to separate the soluble protein from the particulate cell fractions. The recombinant HbI and HbI mutants carrying the His tag were purified using a Co^{2+} affinity column (Talon, Invitrogen). Further purification was achieved by FPLC in a Hi-Load 26/60 Superdex 200 gel filtration column. The purified proteins were concentrated, and the buffer was exchanged by
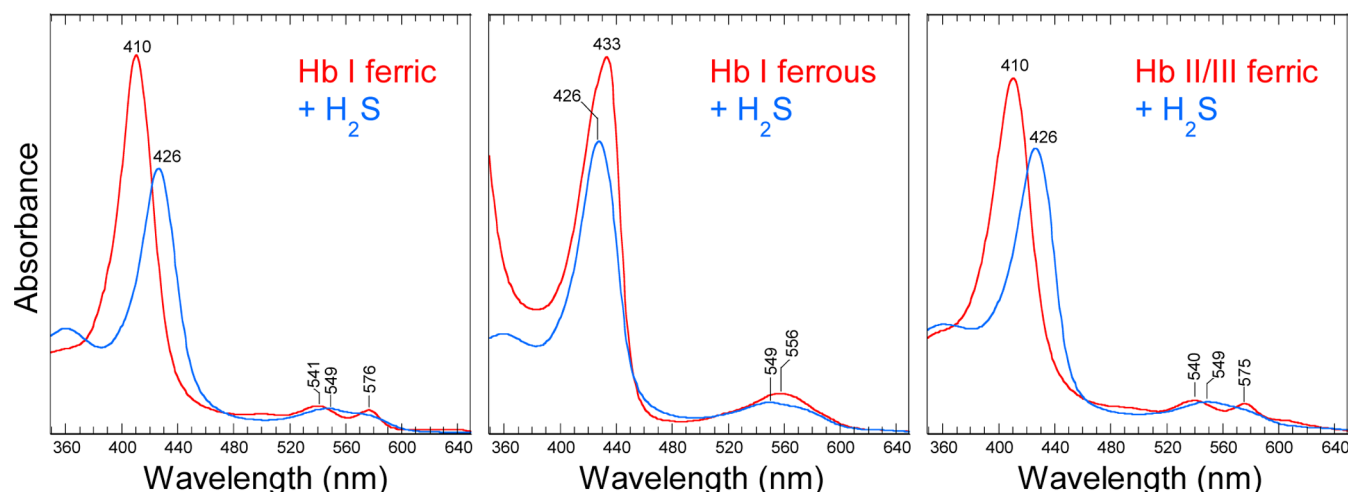
Figure 2. Steady-state absorption spectra of unliganded ferric and ferrous HbI, HbI liganded with H_2S, and ferric HbII/III liganded with H_2S.

ultrafiltration (Millipore) under a N_2 atmosphere. The purity was verified by SDS−PAGE.

Preparation of Samples for Spectroscopy. Purified ferric proteins were dissolved in phosphate buffer (pH 7.4) to ~30 μM, and 100 μL of a solution of proteins was placed in a 1 mm optical path-length quartz cell sealed with a rubber stopper and degassed by means of four successive cycles of vacuuming and purging with argon (Air Liquide, 99.999%). To obtain ferrous species, the ferric proteins were reduced by the addition of 10 μL of a degassed stock solution of sodium dithionite ($Na_2S_2O_4$) or sodium ascorbate (both at a final concentration of 2 mM) in the UV−vis cell. For preparing NO-liganded proteins, the argon gas phase was replaced with a 10% NO gas phase diluted in N_2, directly introduced into the spectroscopic cell still connected to the gas train (at ~1.3 bar) to ensure an "infinite reservoir" of NO during binding equilibration. For the O_2-liganded protein preparation, a small amount of air with a gastight syringe was used after degassing. H_2S-liganded proteins were prepared by the addition of 10 μL of a degassed sodium sulfide (Na_2S) solution to the cell with a gastight syringe (final concentration of 1 mM). The molar concentration ratio between H_2S and protein was ~3. Equilibrium spectra were recorded at each step of the preparation to verify the state of the samples.

Time-Resolved Absorption Spectroscopy. Femtosecond absorption spectroscopy was performed with the pump−probe laser system previously described.[25] The setup provides an excitation pulse at 564 nm in the Q-bands of the heme (duration of ~50 fs, repetition rate of 30 Hz) for photoexcitation. The amplified pulse at 615 nm (duration of 50 fs) produces a pulsed white light continuum after focusing in an 8 mm cell containing pure H_2O. From this continuum, the probe pulse wavelength is selected by a line of two prisms also used for pulse compression. Both beams were focused and spatially overlapped in the sample cell, which was continuously moved in a direction perpendicular to the beams for ensuring sample renewal between laser shots. Transient spectra were recorded simultaneously with kinetics by a CCD detector as a time−wavelength matrix of induced absorption. The CCD calibration was performed with a multiline interference filter. The global analysis of the data was performed by singular-value decomposition (SVD) of this time−wavelength matrix of Soret band absorption changes over the entire recorded time range.[25] From the orthogonal components of this matrix,

decay-associated spectra (DAS) corresponding to one particular exponential decay can be calculated. Alternatively, if the induced signals strongly overlap, analysis of kinetics was also performed at single particular wavelengths. Equilibrium spectra were recorded with a Shimadsu 1700 spectrometer. The accuracy for wavelength determination is ±0.3 nm for steady-state measurements and ±1 nm for transient spectra. All measurements were performed at 20 ± 2 °C.

■ **RESULTS**

The steady-state spectra of HbI in ferric and ferrous states, unliganded and liganded with H_2S, are displayed in Figure 2. The ferric forms of HbI and HbII/III have a Soret maximum positioned at 410 nm, characteristic of a six-coordinate iron with water bound ("aquo-met"). Binding of H_2S to both ferric and ferrous Hbs shifts the maximum of the Soret band to 426 nm, a position clearly different from that of ferrous Hbs liganded with O_2 (414−416 nm).

Before investigating the physiologically relevant dynamics of the distal ligands H_2S, NO, and O_2, we measured the absorption kinetics induced by photoexcitation of unliganded proteins in both redox states. This is necessary because the excited-state relaxation also occurs in the presence of any ligand and must be taken into account in the analysis of heme−ligand interaction in the picosecond range. Then, the excited-state relaxation can be easily distinguished from the dynamics of photodissociated ligand in the transient spectra of liganded Hbs. We performed a global analysis of the evolving transient spectra by means of singular-value decomposition of the time−wavelength matrix,[25] which allowed us to separate spectral and kinetic contributions from several processes.

Unliganded Ferrous and Ferric WT HbI. The excitation of unliganded ferrous HbI produced a red shift and a broadening of the Soret absorption band in the transient spectra (Figure S1 of the Supporting Information). Two processes were identified: vibrational relaxation[25,26] of the excited heme with a τ_{vib} of 3.8 ps and partial photo-oxidation (15% of photoexcited hemes) followed by back-reduction with two time constants (τ_{red} = 6.4 and 280 ps), which correspond to back-electron transfer leading to the reduction of the heme as depicted in Scheme S1 (see the Supporting Information for the full discussion of these processes). The ability of electron transfer from electronically excited heme Fe^{2+} depends on its
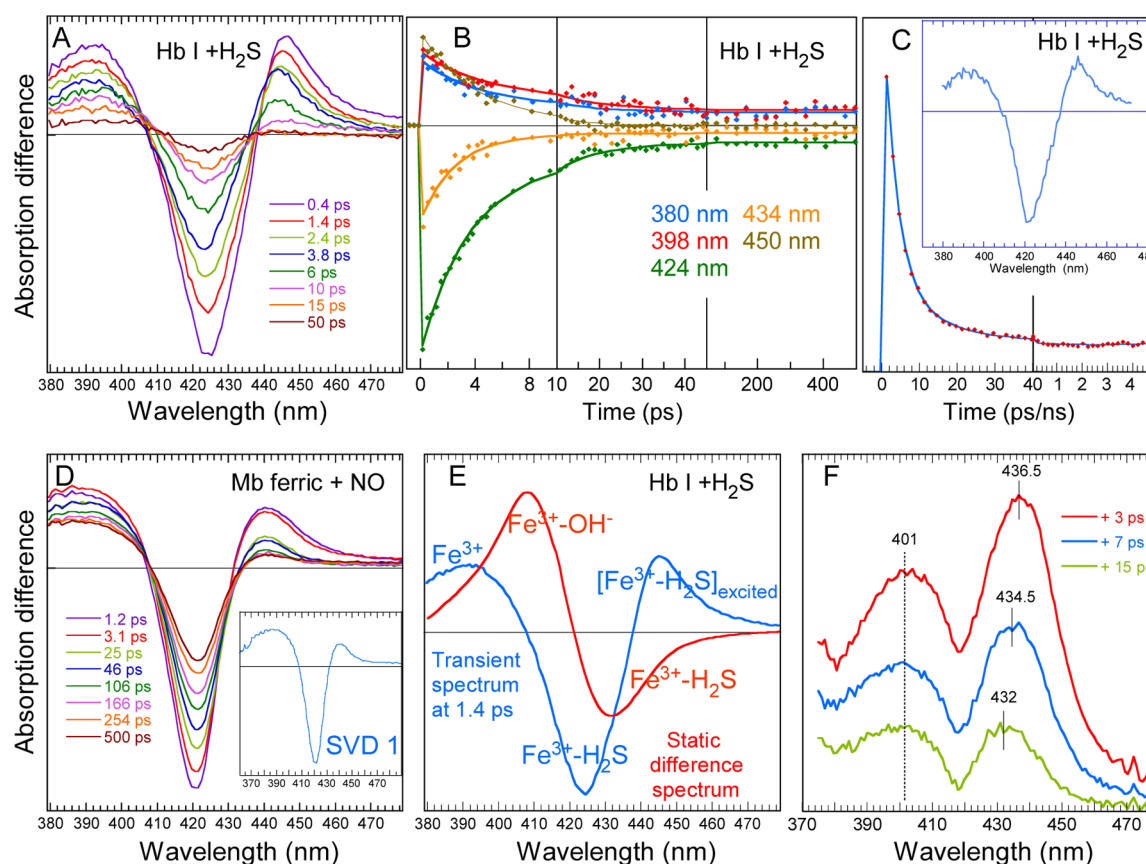
Figure 3. Ferric HbI liganded with H_2S at pH 7.5. (A) Raw transient spectra of HbI at particular time delays after photoexcitation. (B) Kinetics after photoexcitation of H_2S-liganded ferric HbI at particular wavelengths and their fitted trace. Fitted parameters are listed in Table 1. (C) Kinetics measured to 5 ns after photoexcitation of the HbI–H_2S complex. The entire kinetics was fit with only two components: τ_{vib} = 3.8 ps, and τ_{gem} = 15 ps. (D) Transient spectra of ferric myoglobin after NO photodissociation (inset shows the main spectral component). (E) Transient spectrum of the HbI–H_2S complex at 1.4 ps compared to the steady-state difference unliganded minus H_2S-liganded ferric HbI spectrum. The induced absorption bands and the bleaching bands are labeled with their respective assignments. (F) Absolute transient spectra of the species generated by photoexciting the ferric HbI–H_2S complex. These spectra were obtained by subtracting the raw spectrum of the HbI–H_2S complex before excitation (at −1 ps) with a weighting coefficient, from the raw transient spectra at given time delays.

environment. We have already observed such photo-oxidation in the case of the isolated heme domain of soluble guanylate cyclase followed by its back-reduction occurring with two time constants.[27] The presence of two time constants for back-reduction strongly suggests that the electron acceptor (A in Scheme S1 of the Supporting Information) is an internal side chain switching between two conformations characterized by different rates of electron transfer, observed as two kinetic components because the side-chain motion is much slower than the electron transfer. The immediate photo-oxidation of ferrous HbI indicates that the electronic nature of the close heme environment can modulate its redox potential.

As for unliganded WT ferric HbI, only vibrational relaxation[25,26] of the heme in the electronic ground state with a τ_{vib} of 3.8 ps is detected (Figure S2 of the Supporting Information), very similar to that measured for Mb.[26,28] The ferric HbI is in the six-coordinate state with a water molecule as the sixth iron ligand (aquo-met), but the bound water molecule does not dissociate upon photoexcitation, like in the case of ferric myoglobin[29] [see also below the comparison with the ferric Mb–NO complex (Figure 3C)]. We did not observe any photoinduced charge transfer for ferric HbI, contrary to the case for ferrous HbI.

Ferric HbI Liganded with H_2S. After photoexcitation of the ferric HbI–H_2S complex (HbI–H_2S hereafter), the

bleaching centered at 425 nm (Figure 3A) is readily assigned to the disappearance of ground-state liganded species whose steady-state Soret absorption is located at 426 nm (Figure 2). Does photodissociation of H_2S occur, or is there only electronic excitation? The shift of the isosbestic point initially located at 438 nm (Figure 3A) indicates the presence of two simultaneous processes. Contrary to most transient spectra, which have a characteristic derivative-like shape, the transient spectrum of HbI–H_2S presents two induced absorption bands centered at 446 and 395 nm, on each side of the bleaching. This unusual shape may suggest a complex behavior. We fit kinetics at particular wavelengths within the bleaching and the two induced absorption bands (Figure 3B). We obtained only two exponential components with similar time constants at all the wavelengths (Table S3 of the Supporting Information), indicating the presence of only two processes. The first time constant (τ_{vib} = 3.4 ± 0.5 ps) is similar to those we have measured for vibrational relaxation for all the heme proteins studied so far. The induced absorption centered at 446 nm at early time (0.4−6 ps) could apparently be assigned to the reduced unliganded heme because of its position; however, it shifts rapidly, as in the case of photoexcitation of unliganded ferric HbI. We have observed such an absorption in the case of ferric mitochondrial cytochrome c, attributed to the vibrationally hot heme, an interpretation supported by transient Raman
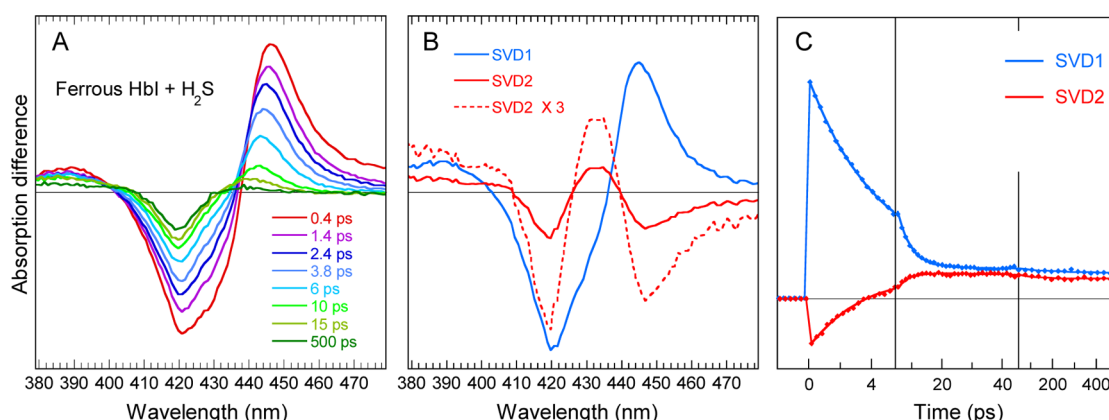
Figure 4. Photodissociation of H_2S from ferrous HbI. (A) Raw transient differential spectra at selected time delays. (B) Spectral components from SVD global analysis and their associated kinetic components (C).

data.[25] Furthermore, the kinetics at 450 nm mainly contains (92%) the contribution of the 3.4 ps component. This induced absorption is therefore assigned to the five-coordinate ferric heme vibrationally excited in the electronic ground state, red-shifted with respect to the Soret band of vibrationally relaxed heme. The bleaching due to photodissociated H_2S truncates the transient spectrum of ferric HbI; because of the strong overlap of bleaching and induced absorption, the SVD global analysis was not efficient in separating them, so we fit the kinetics at single wavelengths.

NO can be photodissociated from the ferric Mb−NO complex, which provides a relevant comparison with ferric HbI−H_2S and whose transient spectrum is shown in Figure 3D. Remarkably, the transient Mb spectrum after NO photodissociation has the same spectral shape, disclosing two induced absorption bands (390 and 440 nm) on each side of the bleaching (421 nm). The absorption of 5-c ferric heme appears as a broad band centered at 391 nm, exactly as in HbI. We thus assigned this induced absorption in HbI to the appearance of the 5-c ferric heme due to the dissociation of H_2S. Importantly, the Soret band is observed at same position in the steady-state spectrum of ferric Mb mutant His(E7)Leu that does not bind water as the sixth iron ligand,[29,30] so that this Soret maximum is characteristic of 5-c ferric b-type heme. The same value (391 nm) was reported for the ferric guanylate cyclase.[31] In the case of WT ferric Mb, the water molecule cannot be photodissociated from the heme, contrary to NO, so that only vibrationally excited heme is obtained in aquo-met Mb.[26] The species ferric 6-c H_2O HbI is not re-formed in the picosecond time range after photodissociation of H_2S, exactly like for the ferric Mb−NO complex,[29] but also for the ferrous Mb−CO complex.[32] This is demonstrated by the comparison between the steady-state difference H_2S-liganded minus unliganded ferric HbI spectrum with the transient spectrum of HbI−H_2S (Figure 3E). The observation of 5-c heme from ferric HbI−H_2S implies that H_2S is photodissociated and H_2S geminately rebinds. Indeed, the decreases in the levels of bleaching and absorption at 395 nm are correlated (Figure 3A). Fitting the kinetics at several wavelengths reveals a very fast monoexponential rebinding of H_2S to the ferric heme (τ_{gem} = 12 ps; 76%). The constant amplitude at 500 ps (∼24%) indicates the proportion of dissociated H_2S that exits the heme pocket. We verified that no further kinetic component exists at a longer time scale after geminate rebinding of H_2S to ferric HbI, as

deduced from the constant absorption up to 5 ns (Figure 3C). A H_2O molecule does not rebind on this time scale.[29,32]

To obtain a better view of the two transient species occurring in the picosecond time range, we have calculated their absolute spectra, obtained by subtracting the raw spectrum of HbI−H_2S before excitation (at −1 ps) with a weighting coefficient from the raw transient spectra at given time delays to remove the bleaching at 424 nm. These coefficients are evolving with time and are proportional to the bleaching evolution, which is given by the expression $0.67 \times \exp(t/3.1\ \text{ps}) + 0.25 \times \exp(t/12\ \text{ps})$ (Table S3 of the Supporting Information) because the decrease in the level of bleaching arises simultaneously from vibrational relaxation and from H_2S rebinding. In Figure 3A, the transient difference spectra were obtained by subtracting the raw spectrum of HbI−H_2S before excitation without any coefficient to reveal the spectral changes. The band at 401 nm is the Soret of unliganded ferric heme, whose amplitude decreases with a time constant of 12 ps. The band shifting from 436.5 to 432 nm is due to the vibrationally excited six-coordinate heme with H_2S still bound. This shift is characteristic of vibrational relaxation with a time constant of 3.1 ps. The complete separation of the two transient Soret bands is not possible, and that of the 5-c heme at 401 nm may contain a contribution from the vibrational excited states.

Ferrous HbI Liganded with H_2S. The photoexcitation of ferrous HbI−H_2S also leads to its dissociation (Figure 4) and is followed by the monoexponential geminate rebinding of H_2S (τ_{gem} = 165 ps) and constant phase, whose relative amplitudes are 20 and 80%, respectively. The affinity of H_2S for ferrous HbI is much lower than for the ferric form,[2] as shown by the presence of a shoulder at 433 nm in the equilibium spectrum (Figure 2) and more conspicuously by a shoulder at 430 nm in the negative band of transient spectra at early times (Figure 4A). This resulted in a larger amplitude of vibrational relaxation of the Fe^{II}−H_2S complex excited states, in comparison with that of ferric HbI−H_2S (Table 1).

Ferric Q(E7) HbI Mutants Liganded with H_2S. To investigate the role of Gln(E7) in the hydrogen bond network,[33] we expressed the two HbI mutants Gln(E7)His and Gln(E7)Val with polar and apolar side chain at position E7(64) in the distal heme pocket for comparison of dynamics of HbI with H_2S with that of WT HbI. Indeed, the Gln(E7)Val variant lacks the ability to form a hydrogen bond at this position. The transient spectra of both mutants after photodissociation of H_2S are shown in Figure 5. First, the shift of the

Table 1. Time Constants and Amplitudes from Fitting the Kinetics after Photoexcitation in HbI and Mutants Liganded with H$_2$S

	H$_2$S geminate rebinding		constant[b]
protein	τ_{gem1} (ps) $(A_1)^a$	τ_{gem2} (ps) $(A_2)^a$	A_3
Fe^{2+} HbI + H$_2$S	–	165 (20)	80
Fe^{3+} HbI + H$_2$S	12 (76)	c	24
Fe^{3+} Q(E7)H + H$_2$S	5.4 (81)	32 (14)	5
Fe^{3+} Q(E7)V + H$_2$S	7.3 (71)	c	29

^{a}Amplitudes A_i are expressed as a percentage of the normalized transient absorption (calculated without the contributions of vibrational relaxation, which are given in Table S2 of the Supporting Information). ^{b}The constant term corresponds to the population not rebinding after 500 ps. ^{c}The quality of the fit was not improved by introducing a second component.

isosbestic point at 430−440 nm is large qualitatively, indicating an important contribution of excited-state relaxation to the transient absorption changes. To quantitate the effect of the mutations, we have fit the kinetics at 424 nm in the bleaching part of the transient spectra to monitor the recovery of the initial H$_2$S-liganded heme. The parameters of the fitted kinetics (Figure 5C) are listed in Table 1.

For the Gln(E7)His mutant, two parameters are changed in comparison with those of WT HbI. First, two components of H$_2$S geminate rebinding are present, with the major one having a very fast time constant (5.4 ps). Second, the population of dissociated H$_2$S that escapes into solution (5%) is much smaller than that for WT (24%). In contrast, only one component is observed for the Gln(E7)Val mutant, which has a larger population of H$_2$S released into solution (29%). Like that of WT, the fit of kinetics for Gln(E7)Val could not be improved by using a second exponential component, whereas that of Gln(E7)His could not be fit with only one component. For both mutants, the induced absorption band below 400 nm is assigned to the 5-c ferric heme, as observed and explained in the case of WT HbI−H$_2$S (Figure 3). Furthermore, the excited-state decay for a ferric heme is usually faster than 5 ps;[25] thus, for the Gln(E7)His mutant, we have assigned the 5.4 ps component to dissociated H$_2$S. However, the very short time

constant (τ_{gem1} = 5.4 ps) implies that dissociated H$_2$S does not move far from the iron before rebinding or that it might be associated with relaxation of the heme−H$_2$S complex in a transient excited vibrational state.

Dynamics of O$_2$ in Ferrous HbI and HbII/III. The equilibrium Soret maximum of the liganded ferrous HbI−O$_2$ complex is located at 416 nm (Figure 6A), similar to that of the Mb−O$_2$ complex, but at 414 nm for Hthe bII/III−O$_2$ complex (Figure S5 of the Supporting Information). The transient spectra of the HbI−O$_2$ complex after excitation (Figure 6B) are similar to those of the Mb−O$_2$ complex (Figure S6 of the Supporting Information). The minimum of bleaching shifts from 414 nm at 0.4 ps to 416 nm because of vibrational relaxation; the position of the minimum is constant after ∼10 ps, and the transient spectra represent only O$_2$ dissociation and geminate rebinding that occurs with two time constants similar to those of the Mb−O$_2$ complex (Table 2). However, the comparison of the transient difference spectrum of the HbI−O$_2$ complex from global SVD analysis (Figure 6D) with the difference of equilibrium spectra (ferrous unliganded minus O$_2$-liganded) reveals a slight shift between both, suggesting that the protein is not in exactly the same state.

As for the isoform of the HbII/III−O$_2$ complex, conspicuous differences are observed (Figure 6C): at 10 ps the amplitude of the difference spectrum decreased much more than in the case of HbI, and there is a shift of the isosbestic point after 10 ps. The kinetics from the global fit is compared with that of HbI (Figure 6F and Table 2). We have calculated the spectra associated with each exponential component [decay-associated spectra (DAS) (Figure 6E)]. The DAS with larger amplitude decays with a time constant of 5.8 ps (72% of the signal) and does not correspond to the steady-state difference "ferrous unliganded minus O$_2$-liganded" spectrum, contrary to the 100 ps and constant DAS that both match this difference. Consequently, the 5.8 ps process cannot be assigned to O$_2$ rebinding, and its origin will be discussed below.

The geminate recombination kinetics of O$_2$ are very different for HbI, HbII/III, and Mb (Figure 6F and Table 2). The fast and slow phases of rebinding of O$_2$ to HbI and Mb occur with the same time constant (τ_{gem1} = 6.0 and 6.3 ps and τ_{gem2} = 396 and 291 ps, respectively) but with different amplitudes.
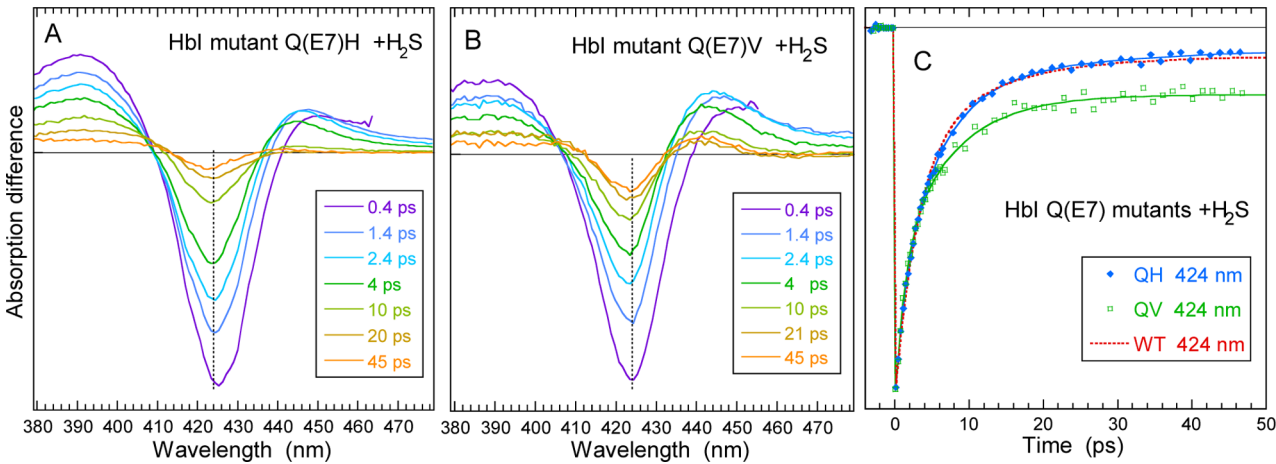

Figure 5. Dynamics of interaction of H$_2$S with the two ferric HbI mutants, Gln(E7)His and Gln(E7)Val. (A and B) Raw transient spectra of mutants Gln(E7)His and Gln(E7)Val, respectively, at particular time delays after photoexcitation. The vertical dotted lines in panels A and B indicate the wavelength (424 nm) at which the kinetics of H$_2$S rebinding are fit. (C) Kinetics of H$_2$S-liganded ferric mutants at the minimum of bleaching and their fitted traces compared with that of WT HbI (red dotted line). The fitted parameters are listed in Table 1.
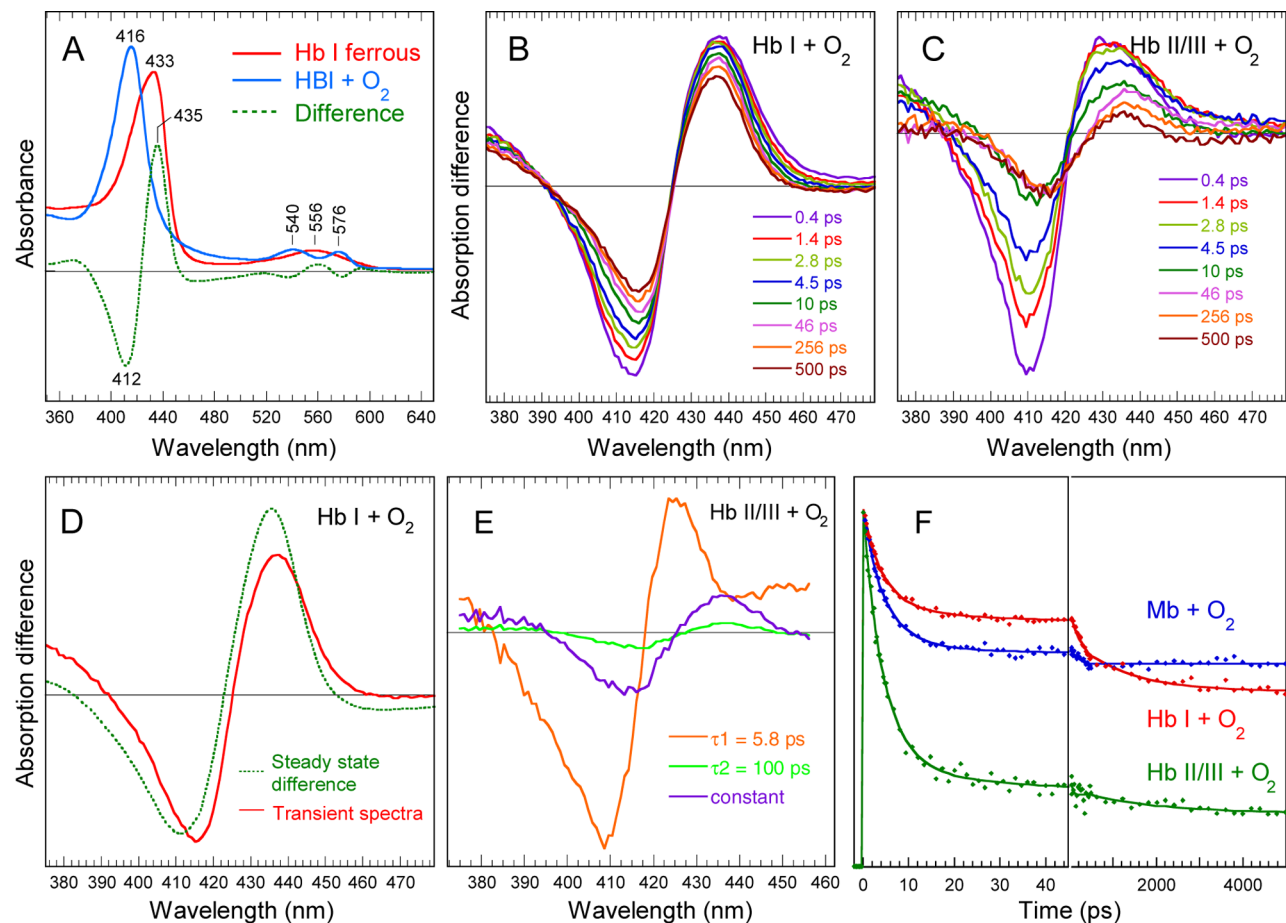
Figure 6. Interaction of O_2 with ferrous HbI, HbII/III, and Mb. (A) Steady-state spectra of unliganded and O_2-liganded ferrous HbI (steady-state spectra of the Mb−O_2 complex and HbII/III are given in Figure S6 of the Supporting Information). (B) Raw transient spectra at various time delays after photoexcitation of ferrous O_2-liganded HbI. (C) Raw transient spectra of ferrous O_2-liganded HbII/III. (D) Transient spectrum of ferrous HbI after O_2 photodissociation compared to the unliganded ferrous minus O_2-liganded HbI steady-state difference spectrum. (E) Calculated transient spectra (DAS) associated with each exponential decay (Table 2) after photoexcitation of the HbII/III−O_2 complex. These DAS were obtained as a linear combination of SVD spectra, from the relative amplitude of the decay in each SVD kinetics. (F) Kinetic components of rebinding of O_2 to ferrous HbI, HbII/III, and Mb up to 5 ns. In the first time window, the kinetics were recorded with a larger time resolution. The fitted parameters are listed in Table 2.

Table 2. Time Constants and Amplitudes from Fitting the Kinetics after Photodissociation of NO or O_2

	geminate rebinding		constant
protein	τ_{gem1} (ps) $(A_1)^a$	τ_{gem2} (ps) $(A_2)^a$	A_3
Fe^{2+} HbI−O_2	6.0 (20.5)	396 (18)	61.5
Fe^{2+} HbII/III−O_2	5.8 (72)	100 (5)	23
Fe^{2+} Mb−O_2	6.3 (28.5)	291 (6)	65.5
Fe^{2+} HbI−NO	8.0 (36)	90 (62)	2
Fe^{2+} HbII/III−NO	11 (83)	61 (15)	2
Fe^{2+} Mb−NO	13 (40)	148 (50)	10
Fe^{3+} Mb−NO	24 (14)	208 (48)	38

^{a}The amplitudes are expressed as percentages of the normalized transient absorption (calculated without the contributions of vibrational relaxation, which are given in Table S4 of the Supporting Information).

Remarkably, the fast rebinding phase for HbII/III (τ_{gem1} = 5.8 ps) has a 3.5-fold relative amplitude compared to the slow phase (τ_{gem2} = 100 ps). The overall amplitude of rebinding of O_2 to HbII/III is much larger with respect to HbI and Mb (77% of dissociated O_2 for HbII/III and 38.5 and 34.5% for HbI and Mb, respectively), revealing a large constraint for the

movement of the ligand away from the heme iron. This will be discussed in view of the respective structure and function of the Hb isoforms.

Dynamics of NO in Ferrous HbI and HbII/III. The dynamics of NO in ferrous HbI and HbII/III were also measured and compared with that of the Mb−NO complex. NO dissociation is immediately identified by the raw transient spectra after NO photoexcitation from HbI (Figure 7B), which are similar to the "unliganded minus NO-liganded" steady-state difference spectra (Figure 7A). The larger spectral component from global analysis (SVD) is due to NO rebinding and is similar for the three proteins (Figure 7C). Like that for other six-coordinate ferrous heme proteins,[34] the geminate NO recombination takes place on the picosecond time range (Figure 7D; fitted parameters listed in Table 2). The overall rebinding of NO to both HbI and HbII/III is almost complete at 500 ps (Figure 7D), so that only 2% of dissociated NO did not rebind (compared to 10% for Mb). As for Mb, NO rebinds to HbI and HbII/III with two geminate phases, the fast one corresponding to NO rebinding without an energy barrier[34,35] and the second being caused by NO having diffused farther into the heme pocket (docking site) so that it encounters a steric energy barrier for rebinding. The fast time constant is similar
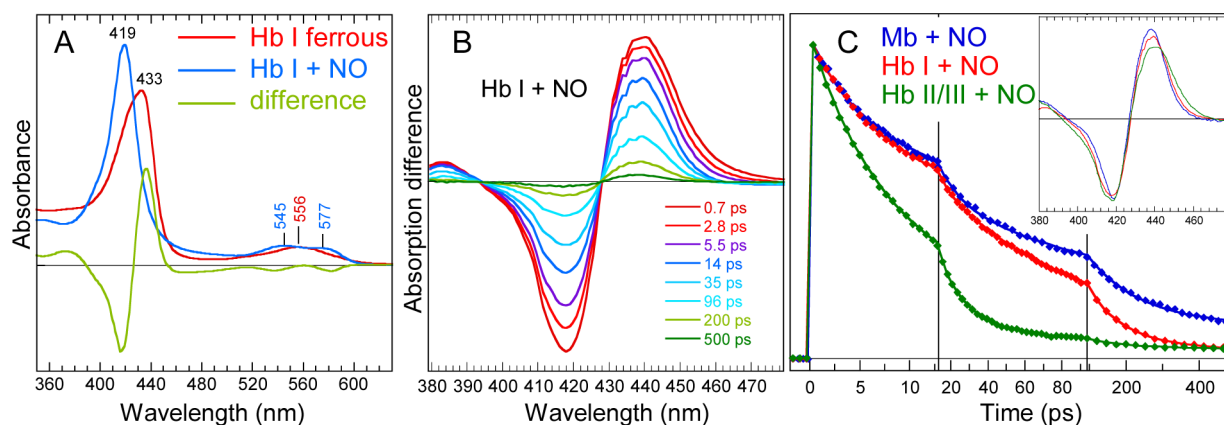
Figure 7. Interaction of NO with ferrous HbI, HbII/III, and Mb. (A) Steady-state spectra of unliganded and NO-liganded ferrous HbI. (B) Raw transient spectra at various time delays after photoexcitation of ferrous NO-liganded HbI. (C) Kinetics of ferrous HbI and HbII/III from global SVD analysis compared to that of Mb after NO photodissociation up to 500 ps. The fitted parameters are listed in Table 2. The inset shows the associated SVD transient spectra of ferrous HbI, HbI/III, and Mb after NO photodissociation.

for all three proteins (τ_{gem1} = 8−13 ps), but their amplitudes differ; the second geminate phase for the three proteins varies in both time constant (τ_{gem1} = 61−148 ps) and amplitude.
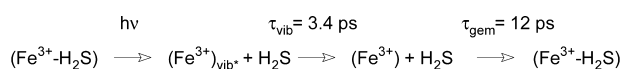
■ DISCUSSION

Photodissociation of H_2S from Ferric WT Hbl. After photoexcitation of ferric HbI−H_2S, an intense induced absorption band appeared at 446 nm, the magnitude of which decreased rapidly (Figure 3A). At first glance, this band could be assigned to the formation of ferrous unliganded HbI, thus to photoreduction. However, several arguments led us to conclude that the main contribution is H_2S photodissociation. First, a similar induced absorption due to the 5-c ferric heme is observed in the case of the ferric dissociated Mb−NO complex (Figure 3C). Second, we can infer that photoreduction did not occur for the following reasons. Fitting the kinetics at 450 nm yielded only two exponential components, the larger one (92%) being due to vibrational relaxation (same time constant as in the absence of H_2S, 3.4 ± 0.5 ps) and the smaller one (8%) being similar (12 ± 1 ps) to that obtained when fitting the kinetics (Table S3 of the Supporting Information) in the bleaching due to H_2S geminate rebinding. Thus, the induced absorption located at 440−460 nm (Figure 3A), i.e., at an energy lower than that of the ground-state Soret band, is assigned to vibrational excited states of the heme, exactly as observed for photodissociated NO from ferric Mb (Figure 3C). We thus conclude that photoreduction did not occur in this case of ferric HbI−H_2S and that the picosecond transient spectra reflect only vibrational relaxation of the heme followed by H_2S geminate rebinding (Scheme 1). The partial reduction of the HbI heme by H_2S followed by sulfide release has been observed before by static resonance Raman under equilibrium conditions.[10] Because no photoreduction was detected here, we infer that the reduction of HbI heme by H_2S occurs on a longer time scale. These transient spectra demonstrate that H_2S can be photodissociated from ferric heme in HbI upon excitation of

the heme in the Q-bands (564 nm), contrary to the case of water bound to the ferric heme of Mb[26] and CN$^-$ bound to the ferric heme of both Mb and HbI,[36] which do not dissociate, even when using a more energetic photon at 405 nm. This indicates different electronic configurations in the excited state for both types of ligands. The contribution of vibrational excited states comes not only from the photodissociated heme but also from nondissociated 6c-H_2S heme. The vibrational excitation of a diatomic ligand bound to the heme without dissociation was also observed in the case of the ferric HbI−CN complex.[36] The photodissociation of the Fe−S bond was also achieved with the same excitation wavelength (564 nm) in ferrous Cyt c whose heme Fe^{2+} is linked to a distal methionine sulfur;[25] however, photodissociation does not occur for ferric Cyt c,[25] contrary to ferric HbI−H_2S.

Geminate Rebinding of H_2S in Ferric WT Hbl. The transient spectra 20 ps and 5 ns after H_2S dissociation are identical, and no transition other than rebinding takes place; in particular, no water molecule binds to the ferric heme on this time scale. Using the amplitude of the kinetic components (with the approximation of similar absorption coefficients), we measured that 20% of photodissociated H_2S escapes from the heme pocket into solvent while 80% of H_2S rebinds to the heme. The geminate rebinding of H_2S to Fe^{3+}-Mb (τ_{gem} = 12 ps) is faster than that of NO (τ_{gem1} = 24 ps, and τ_{gem2} = 208 ps). Two factors may explain this fact. First, for ionizable ligands interacting with ferric heme (H_2O/OH^- and H_2S/SH^-), the electrostatic potential favors ultrafast ligand rebinding. Second, H_2S forms a hydrogen bond that precludes its diffusion and holds it in place.

Immediately after photodissociation, the iron is positioned out of the heme plane ∼0.3 Å toward the proximal His.[34] Because H_2S rebinds to ferric HbI as fast as NO binds to ferrous Mb (τ_{gem} = 12 ps), a process that is barrierless for NO,[34,35] we infer that H_2S rebinds whatever the position of Fe^{3+} with respect to the heme plane. Thus, there does not exist any energy barrier for the rebinding of H_2S to Fe^{3+}. In ferric Mb as well as ferrous Mb, the geminate rebinding of NO occurs with two phases (Table 2). Contrary to Mb[34] and NO synthases,[37] which have two and three NO geminate phases, respectively, there exists only a single phase of geminate recombination in HbI−H_2S, with a constant term (20%) corresponding to the escape of photodissociated H_2S to the

Scheme 1. Processes Photoinduced in Ferric HbI−H_2S^{a}

$$\text{(Fe}^{3+}\text{-H}_2\text{S)} \xrightarrow{h\nu} \text{(Fe}^{3+}\text{)}_{vib^*} + \text{H}_2\text{S} \xrightarrow{\tau_{vib} = 3.4 \text{ ps}} \text{(Fe}^{3+}\text{)} + \text{H}_2\text{S} \xrightarrow{\tau_{gem} = 12 \text{ ps}} \text{(Fe}^{3+}\text{-H}_2\text{S)}$$

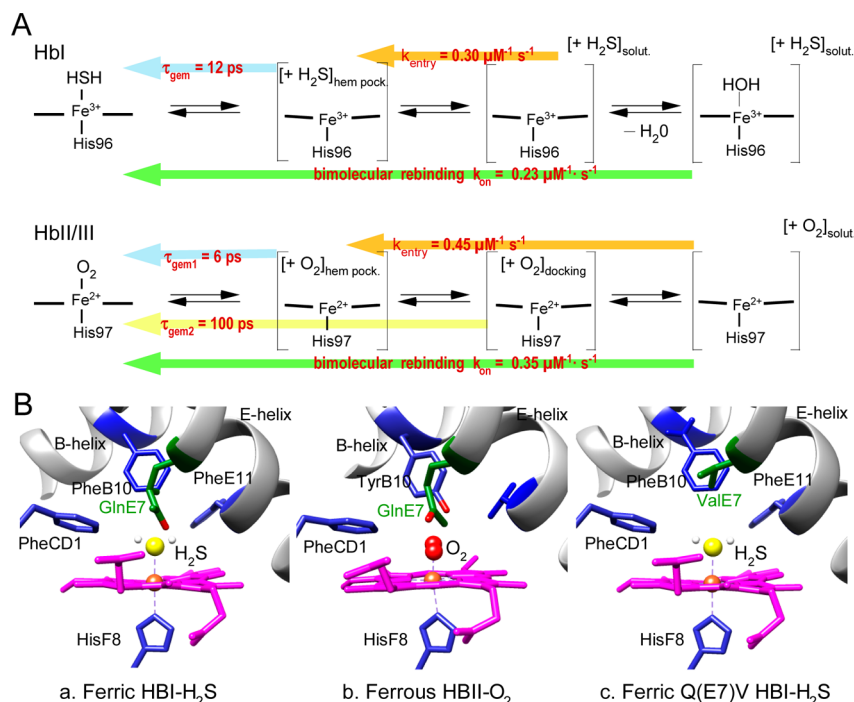^{a}vib* represents the vibrational excited state.

Figure 8. (A) Correspondence between the measured time constants and the rebinding of H_2S and O_2 to the heme from different positions of the ligands with respect to the protein: in the heme pocket, in the docking site, and in the solvent. For H_2S, there is no docking site, contrary to the case for O_2. Contrary to ligand binding from the solvent, the other phases involve the same molecule that was photodissociated. (B) Detailed illustrations of the ligand interactions in the heme cavity for (a) ferric HbI−H_2S, (b) the ferrous HbII/III−O_2 tetramer, and (c) the ferric Q(E7)V HbI−H_2S mutant. The position of the Val side chain in the structure of the Q(E7)V mutant was determined with Chimera.[66]

solvent. Consequently, there is no docking site for H_2S, contrary to the case for NO, and the only energy barrier resides between the solvent and the heme pocket, which can be modulated by distal side chains.[38−40]

The structure of H_2S-liganded HbI revealed that the sulfur atom participates in a hydrogen bond with the side chain of Gln(E7) (Figure 8) and that three side chains, Phe29(B10), Phe43(CD1), and Phe68(E11), are favorably positioned to stabilize H_2S through aromatic−electrostatic interactions, forming what has been called a "Phe cage".[40] The effect of this very particular structure is to restrain the H_2S dynamics, favoring its rebinding. Thus, the high yield of H_2S rebinding explains its very slow rate of dissociation (2.2×10^{-4} s^{-1}) from ferric HbI, supporting the fact that H_2S release is facilitated by heme reduction.

The photodissociation of H_2S also occurs in the ferrous HbI−H_2S complex (Figure 4), and its geminate rebinding is also monoexponential but with a larger time constant (165 ps; 20%) and a larger constant phase whose relative amplitude represents 80% of photodissociated H_2S. Importantly, these proportions are inverted with respect to the ferric form (Table 1). The constant phase corresponds to H_2S that escaped into solution, and its amplitude is directly correlated with the affinity of H_2S, which is lower for ferrous HbI. The slow geminate phase for the ferrous species (τ_{gem} = 165 ps) indicates a higher energy barrier for rebinding, only because of the ferrous state of the heme. This observation is in line with the binding of H_2O to ferric Mb and not to ferrous Mb, given the similar electronic configuration of sulfur and oxygen atoms (four electrons in the external p subshell). The existence of a single phase for H_2S rebinding in both ferric and ferrous HbI, despite a large difference in affinity between both, confirms that only an

energy barrier due to steric constraints resides between the distal pocket and the solvent.

H_2S Exiting the Heme Pocket and the H-Bond Network in Ferric HbI. Several side chains within the distal pocket of HbI are involved in a hydrogen bond network,[33,41] especially Gln(E7), whose mutation alters the properties of the protein.[10] The kinetic parameters of H_2S geminate rebinding are changed upon mutation of Gln(E7) (Table 1): the proportion of H_2S released into solution is increased for the Gln(E7)Val mutant (29%) but decreased substantially for the Gln(E7)His mutant (5%). For the latter, a fast component (τ_{gem1} = 5.4 ps) appeared with a high amplitude (81%). Remarkably, the Gln(E7)His mutation induced an increase in the rates of association of both O_2 and CO but a decrease in this rate for H_2S.[10] This suggests the presence of a strong hydrogen bond between His and the bound H_2S, which slows its escape to the solvent. In the Gln(E7)Val mutant, the lack of hydrogen bonds facilitates ligand escape. These findings are consistent with the observed reduction of the ferric heme by H_2S in these variants.[10] In this regard, it has been suggested that heme reduction is facilitated by a strong hydrogen bond between His and the bound H_2S, while the lack of this interaction in the Gln(E7)Val mutant decreases significantly the extent of heme reduction. Thus, it appears that the reduction of ferric heme by H_2S is correlated to H_2S dynamics through the hydrogen bond network that holds it in place.

Furthermore, in the Gln(E7)His mutant, the main absorption change occurs with a time constant of 5.4 ps, accounting for 81% of H_2S dynamics, which is faster than usual geminate rebinding. This of value τ_{gem1} (5.4 ps) implies that photoexcited H_2S must stay in very close to the iron. Because the vibrational relaxation of the heme was taken into account by a 1.3 ps component when fitting the kinetics (Table S2 of the

Table 3. Association Rates, Dissociation Rates, and Dissociation Constants for Binding of a Ligand to HbI and HbII/III Compared to Those of Mb and Hbs from Invertebrates[a]

protein–ligand[b]	B10/E7[c]	conditions[d]	k_{on} (μM^{-1} s^{-1})	k_{off} (s^{-1})	K_D (μM)	ref
Fe^{3+} HbI–H_2S		pH 7.5; 20 °C	0.23	2.2×10^{-4}	10^{-3}	2
Fe^{3+} HbII/III–H_2S		pH 7.5; 20 °C	0.011	1.7×10^{-2}	1.5	2
HbI–O_2	F/Q	pH 7.5; 20 °C	100–200	61	0.3–0.6	2
HbI–O_2 mutant	F/H	pH 7.4; 25 °C	31	3	0.1	10
HbI–O_2 mutant	Y/Q	pH 7.4; 25 °C	6.8	0.6	0.09	10
HbII/III–O_2	Y/Q	pH 7.5; 20 °C	0.35	0.11	0.3	2
Cl TrHb–O_2[e]	Y/Q	pH 7.0; 20 °C	230	190	0.8	9
As TrHb–O_2[f]	Y/Q		1.5	4×10^{-3}	2.7×10^{-3}	51
Mt TrHbN–O_2[g]	Y/L	pH 7.5	55	0.2	8×10^{-3}	55
Mt TrHbO–O_2[g]	Y/A	pH 7.5; 23 °C	0.11	1.4×10^{-3}	1.3×10^{-2}	54
Sw Mb–O_2 mutant	Y/Q	pH 7.0; 20 °C	2.8	1.6	0.6	40
Sw Mb–O_2 WT	L/H	pH 7.0; 20 °C	17	15	1.1	40
horse heart Mb–O_2	L/H	pH 7.0; 25 °C	22	24	1.1	63
HbI–NO		pH 7.0; 25 °C	109	4×10^{-4}	3.7×10^{-6}	33
HbII/III–NO		pH 7.0; 25 °C	2.4	7.1×10^{-4}	3×10^{-4}	33
horse heart Mb–NO			17	1.2×10^{-4}	0.7×10^{-5}	64
sperm whale Mb–NO		pH 7.0; 20 °C	22	1×10^{-4}	0.45×10^{-5}	65

[a]Values for other proteins can be found in the cited references. [b]Proteins liganded with O_2 and NO are all in the ferrous state. [c]Pair of side chains within the heme pocket. [d]Hydrogen sulfide acts as a weak acid with a pK_a of 6.9 at 18 °C (at 0.01–0.1 M), giving the hydrosulfide ion HS^-. [e]Truncated hemoglobin from *Cerebratulus lacteus*. [f]Hemoglobin from *Ascaris suum*. [g]Truncated hemoglobin from *Mycobacterium tuberculosis*, type N or type O. For TrHbO–O_2, there is another minor component (20%) for both k_{on} and k_{off}.

Supporting Information), we consequently assigned the 5.4 ps component to the relaxation of the heme–H_2S complex in a transient excited vibrational state, H_2S still being bound to Fe^{3+}. This particular six-coordinate excited complex decays to the relaxed ground state with a time constant (5.4 ps) very close to that observed in the case of ferrous heme in the O_2 sensor Dos[42,43] and the truncated hemoglobin Mt-TrHbO.[44] Accordingly, we suggest that the six-coordinate vibrationally excited heme–H_2S transient species is due to the trapping of H_2S by hydrogen bonds. Thus, for the Gln(E7)His variant, only a τ_{gem2} of 32 ps corresponds *stricto sensu* to H_2S geminate rebinding, which is slower than in the case of WT and Gln(E7)Val HbI but with a small amplitude (14%). Data for H_2S dynamics in other proteins are not yet available, and we may attempt a comparison with those of other ligands, if not considering their bonding with the iron. The human Mb variant His(E7)Gln, carrying a mutation that is the reverse of what we have performed in HbI, was shown to disclose a faster NO geminate recombination (9 ps) than WT human Mb (24 ps),[45] in agreement with our observations of HbI variants and H_2S (Table 1). This may indicate a general role of distal His(E7) with ligands able to form a hydrogen bond. In summary, the dynamics in Gln(E7)His HbI suggest that the strong H-bond between H_2S and His limits H_2S photodissociation (only 19% is photodissociated) and ligand escape (5%), contrary to the case for Gln(E7)Val HbI in which 29% migrates to the solvent. Photodissociated H_2S can still participate in favorable electrostatic interactions and hydrogen bonds. The faster rebinding in Gln(E7)Val HbI with respect to that in WT HbI can be explained by the lack of a hydrogen bond interaction of the photodissociated H_2S with the apolar Val, which eliminates one internal barrier for ligand recombination. In the Gln(E7)His and WT HbI variants, the interaction of the photodissociated and diffusing ligand with their polar side chains slightly increases the barrier of H_2S rebinding from the distal pocket to the iron. Moreover, the existence of a single geminate rebinding process for the three HbI variants confirms that only one

energy barrier resides in the distal pocket and that there is no "docking site" for H_2S.

Major Species in the Photoexcited HbII/III–O_2 Complex versus the HbI–O_2 Complex. The shape and evolution of the transient spectra shortly after photoexcitation of the HbII/III–O_2 complex are remarkably different from that of the HbI–O_2 complex (Figure 6B,C). In the time interval of 10–50 ps, the isosbestic point shifts from 422 to 427 nm, a direction that is the opposite of that observed in the case of vibrational relaxation of ferrous heme.[25] Consequently, this shift cannot be due to vibrational relaxation of the 5-c heme, which was taken into account by a 2.7 ps component in the fitted kinetics (Table S4 of the Supporting Information). The absorption decrease at 430 nm occurs simultaneously with this shift with a time constant of 5.8 ps and represents 72% of the signal. Considering that the transient difference spectrum associated with the 5.8 ps decay does not match that of the steady-state difference "O_2-liganded minus unliganded" HbII/III spectrum (Figure 6D) and that its time constant is slower than thermal relaxation but faster than geminate rebinding, we assigned this phase to the relaxation of the heme–O_2 complex in a transient excited vibrational state with O_2 still bound to Fe^{2+}. This phenomenon is the same as the one we observed with the photoexcited mutant Gln(E7)His–H_2S complex (*vide supra*). This six-coordinate excited species decays to the ground state with a time constant (5.8 ps) similar to that observed in the case of the O_2 sensor Dos[42] and very close to that of the truncated hemoglobin Mt-TrHbO[44] and the O_2 sensor FixL (4.7 ps),[42] for which no heme doming is observed after photoexcitation.[43] The 5.8 ps time constant, first assigned to O_2 geminate rebinding in the O_2 sensor DOS,[41] was later reassigned to the six-coordinate vibrationally excited heme–O_2 complex on the basis of time-resolved Raman spectra,[43] a transient species that is induced by the trapping of O_2 by hydrogen bond(s) in a configuration still interacting with Fe^{2+}. Consequently, only O_2 that rebinds with a τ_{gem} of 100 ps corresponds to geminate rebinding *stricto sensu*, and the

Table 4. Rate Constants k_{entry} and k_{exit} Calculated from the Experimental Values of $\langle k_{gem} \rangle$, A_{gem}, and k_{on}

	geminate rebinding[a]		ligand diffusion		
protein	$\langle k_{gem} \rangle$ (s^{-1})	A_{gem}	k_{entry} ($\mu M^{-1}\,s^{-1}$)	k_{exit} (s^{-1})	association constant k_{on} ($\mu M^{-1}\,s^{-1}$)
Fe^{3+} HbI–H_2S	0.83×10^{11}	0.76	0.30	0.2×10^{11}	0.23
Fe^{2+} HbI–O_2	0.53×10^{10}	0.385	260–520	0.33×10^{10}	100–200
Fe^{2+} HbII/III–O_2	0.84×10^{11}	0.77	0.45	0.2×10^{11}	0.35
Fe^{2+} Mb–O_2[b]	0.18×10^{11}	0.345	64	0.12×10^{11}	22
Fe^{2+} HbI–NO	0.17×10^{11}	0.98	111	0.3×10^{9}	109
Fe^{2+} HbII/III–NO	0.54×10^{11}	0.98	2.45	0.11×10^{10}	2.4
Fe^{2+} Mb–NO[b]	0.11×10^{11}	0.90	18.9	0.11×10^{10}	17

[a]$\langle k_{gem} \rangle$ is calculated from the weighted time constants of the two geminate rebinding phases. [b]Horse heart myoglobin.

quantum yield for O_2 dissociation is much lower for the HbII/III–O_2 complex than for the HbI–O_2 complex. The constant of 23% corresponds to the O_2 population not rebinding, which was shown not even to rebind up to ~2 μs.[33]

The partial negative charge of bound O_2 can be involved in hydrogen bonds with donors such as Tyr(B10) or His(E7) or can interact with the delocalized partial charge of aromatic rings. Once the Fe–O_2 bond is broken, the ligand becomes neutral and no favorable electrostatic interaction occurs. Thus, in the vibrationally excited Fe^{2+}–O_2 complex, the ligand can still be held in a bound position whereas dissociated O_2 only sterically interacts with distal side chains. The occurrence of the six-coordinate excited species, greatly decreasing the dissociation yield, is correlated with hydrogen bonding that stabilizes O_2 bound to the heme Fe^{2+}. Whereas Mt-TrHbO possesses a distal Tyr(B10)[44] like HbII/III does, in the case of the O_2 sensors Dos and FixL, a distal Arg side chain forms a hydrogen bond with O_2.

Dynamics of O_2 in *Lucina* HbI and HbII/III. First, a spectral observation addresses the structural change in HbI. The transient difference spectrum associated with the geminate rebinding of O_2 to HbI does not match the equilibrium difference spectrum but is slightly shifted (Figure 6D). This was also observed in the case of the O_2 sensors DOS and FixL[42] and reveals that within 5 ns of O_2 dissociation the protein conformation has not yet relaxed to its equilibrium unliganded state. Consequently, a conformational transition of the heme takes place after a delay of >5 ns following Fe^{2+}–O_2 bond breaking.

As deduced from the presence of two geminate phases, O_2 diffuses into a docking site in *L. pectinata* Hbs, contrary to the ligand H_2S (Figure 8A). As opposed to HbI, the much faster and complete rebinding of O_2 in the case of HbII/III (Figure 6F) reveals a higher energy barrier to be overcome for O_2 diffusing out of the heme pocket, which explains the 554-fold lower k_{off} for HbII/III (0.1 s^{-1}) compared to that of HbI (61 s^{-1}) (Table 3). The ratio of k_{on} between isoforms HbI and HbII/III is of the same order of magnitude as the ratio of k_{off}, yielding dissociation constants (3×10^{-7} M) remarkably close for both. However, there is a very large difference in amplitude between the geminate rebinding components in HbI and HbII/III (Table 2) and thus a large difference in the energy barriers for O_2 entering and escaping the heme pocket. The ferrous HbI–O_2 complex has a large association rate ($1-2 \times 10^8$ M^{-1} s^{-1}) that is close to the diffusion limit,[2,46,47] in line with a low energy barrier for O_2 accessing the heme pocket. This energy barrier influences O_2 dynamics in both directions (from and toward the distal heme pocket) and thus is the origin of the decrease in both k_{off} and k_{on} for HbII/III compared to those of HbI. The HbII structure[38] revealed that its heme group is

buried farther than in HbI and that O_2 is tightly liganded through hydrogen bonds with residues Gln(E7) and Tyr(B10), the latter being present only in HbII/III and replaced by Phe in HbI. Is the substitution of Phe for Tyr at the B10 position sufficient for eliciting faster geminate rates and thus modifying the association and dissociation kinetics? To mimic the HbII/III distal pocket, we previously replaced Phe(B10) with Tyr in HbI and observed that both O_2 k_{on} and k_{off} rates decreased by factors of 28 and ~100, respectively.[10] Despite the same B10/E7 pair, the HbI Phe(B10)Tyr mutant O_2 off rate is still 6 times larger than in HbII/III, indicating that other factors are contributing to O_2 dynamics. As described next, this is further supported by comparing the HbII/III–O_2 binding rates with those of other hemoglobins and several myoglobin mutants (Tables 3 and 4).

From the experimental parameters of geminate rebinding, its rate, k_{gem}, and its normalized amplitude, A_{gem}, it is possible to obtain the rates of entry and exit of the ligand (k_{entry} and k_{exit}, respectively) from the solvent to the distal heme pocket, which quantifies the heme accessibility for comparison with other invertebrate Hbs. This is possible from our data provided that no other geminate component exists on longer time scales (10 ns to 10 μs). A previous study showed that HbII geminate rebinding on the nanosecond to microsecond time scale[33] occurs neither for CO nor for O_2, contrary to Hb from *Ascaris suum*, which showed a geminate phase of ~50 ns for O_2. The picosecond geminate phase in the kinetics of the HbII–O_2 complex was not detected with an 8 ns laser pulse,[33] and the constant amplitude of these previous kinetics must correspond to the 23% constant phase that we have measured. As for the ferrous Mb–NO complex, no kinetics on the 10 ns to 1 μs time scale was reported so far, and the calculation of k_{entry} in this case is subjected to the hypothesis that no long geminate phase exists. However, we calculated k_{entry} for ferric HbI–H_2S because we did not observe any process in the 1–5 ns time range, acknowledging the possibility of a much longer phase but with a very small amplitude. In the case of the Hb–O_2 complex, we considered the position of unbound O_2 either in the distal pocket or in the docking site as a single intermediate state. Consequently, for determining k_{entry}, we have used the simplified model[9,48] described in Scheme 2 for which
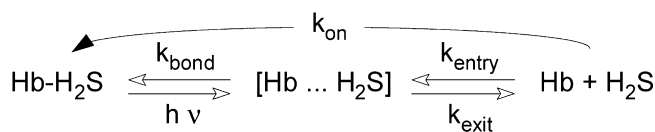
$$A_{gem} = k_{bond}/(k_{bond} + k_{exit})$$

$$k_{gem} = k_{bond} + k_{exit}$$

$$k_{on} = (k_{entry}k_{bond})/(k_{bond} + k_{exit}) = k_{entry}A_{gem}$$

$$k_{exit} = k_{gem} \times (1 - A_{gem})$$

Scheme 2

For each species, k_{gem} is obtained by first calculating an average time constant from the weighted time constants of the two geminate rebinding phases. The values of k_{entry} and k_{exit} are listed in Table 4. It must be noted that, as calculated, k_{exit} represents the depletion of free ligand in the heme pocket caused by geminate rebinding and not the ease with which the ligand moves into the exit channel.

Role of the Distal Side Chains Compared in *Lucina* and Other Invertebrate Hemoglobins. To evaluate the structural factors controling O_2 kinetics in HbII/III, we compared the O_2 binding rates of *L. pectinata* Hbs with those of several invertebrate hemoglobins and of Mb mutants at positions E7 and B10, which resembles the HbII/III distal cavity. In this comparison, we will consider steric restrictions by side chains for diffusion of O_2 from and to the iron, modulating the geminate rebinding probability and its entry in the heme pocket. In all cases, the reactivity of the iron atom itself is identical, because the geminate rebinding of O_2 is as fast as that of NO, meaning that it does not depend on the in-plane iron movement.[34,35] The comparison of the rates is correlated with the structure of these various proteins.

Intriguingly, the Leu(B10)Tyr mutation in sperm whale myoglobin greatly increases the O_2 k_{off} rate (500-fold) and induces two k_{on} rates (first k_{on} is unchanged, and the second is 10-fold lower),[49] whereas the Leu(B10)Phe mutation decreases k_{off} without affecting k_{on}.[50] This behavior is contrary to that observed when considering only the B10 side chain and comparing HbI with HbII/III. The His(E7)Gln single mutation in Mb increases k_{off} (10-fold), but the double mutation of the B10/E7 side chains from Leu/His to Tyr/Gln decreases both the k_{on} and k_{off} rates[51] (Table 3). This illustrates the important fact that contributions from distal side chains are not merely additive and that the hydrogen bonding pattern and steric barrier must be considered within each particular protein structure and cannot be generalized, even within the same globin fold. Thus, whereas the stabilization of O_2 by hydrogen bonding to Tyr(B10) qualitatively explains the more efficient O_2 trapping in HbII/III compared to that in HbI, other structural features must modulate O_2 migration and contribute to the decrease in both k_{on} and k_{off}. In fact, heme proteins that possess the Gln(E7)/Tyr(B10) pair disclose k_{off} values, which span several orders of magnitude from 4×10^{-3} to 24 s^{-1}, and comparison is made with other Hbs (Table 3).

The truncated Hb from the sea worm *Cerebratulus lacteus* (*Cl*-TrHb) possesses Tyr(B10) and Gln(E7) in its binding site,[9] as seen for HbII/III, but has a much larger k_{off} (1730 times) and k_{on} ($\times 660$ times) yet has a K_D for O_2 that is only 2.6 times larger than that of HbII/III (Table 3). On the other hand, HbI possesses Phe(B10) and has binding rates much closer to those of *Cl*-TrHb than those of HbII/III. The effect of the distal Tyr(B10) may be opposite in different Hbs. In *Chlamydomonas* Hb,[52] bound O_2 is stabilized by a hydrogen bond with Tyr(B10) and its replacement with Leu induces a 70-fold increase in k_{off} whereas in *C. lacteus* Hb, the Tyr(B10) hydroxyl group electrostatically destabilizes bound O_2 because of the presence of the neighboring Thr(E11).[9] Consequently,

Tyr(B10) is not the only determinant of O_2 binding. Indeed, the hemoglobin from *A. suum* is the globin with the highest O_2 affinity ($K_D = 2.7$ nM) because of its low k_{off}[53] explained by a synergistic effect of both side chains of the distal Tyr/Gln pair providing an additional hydrogen bond to O_2.[53] The photodissociation of O_2 from *As*-TrHb produces a very high amplitude of geminate rebinding (>99%; time constant of <20 ps, albeit not resolved),[49] which accounts for its low k_{off} and is in qualitative agreement with our measurements for HbII/III (72%; 5.8 ps). In HbII/III, the strong hydrogen bonds between the pair of Tyr(B10) and Gln(E7) side chains and bound O_2 also act in synergy to increase the level of O_2 geminate recombination, resulting in a decreased k_{off}. Nonetheless, these polar interactions vary within proteins having the same Tyr(B10)/Gln(E7) motif, modulating the ligand kinetics.

The truncated Hbs from *Mycobacterium tuberculosis* type N or type O have the intermediate (0.2 s^{-1}) and lowest k_{off} (1.4 × 10^{-3} s^{-1})[54] for O_2, respectively (Table 3 and references cited therein). *Mt*-TrHbO, whose E7 side chain is Ala, is remarkable because it discloses at the same time the lowest k_{off} and the lowest k_{on}, resulting in a K_D 5 times larger than that of *As*-TrHb but only 1.6 times larger than that of *Mt*-TrHbN. Thus, in *Mt*-TrHbs, the substitution of Leu(E7) for Ala(E7) increases both k_{on} and k_{off}, showing that steric hindrance plays a major role. The geminate rebinding of O_2 to *Mt*-TrHbO proceeds in two phases with very fast time constants (4.8 ps, 92%; 20 ps, ~7%).[44] The major and very fast component is in line with our observations (5.8 ps, 72%) for the HbII/III−O_2 complex, assigned to hold O_2 in place by hydrogen bonding. However, the difference in the geminate rebinding amplitude between HbII/III and *Mt*-TrHbO (77 and 99%, respectively) accounts for their difference in k_{off} despite their identical Tyr(B10), which is thus not the only factor for holding O_2 in a bound position. Conversely, Tyr(B10) contributes to the energy barrier to O_2 binding: the k_{on} rate is decreased 15-fold by the Phe(B10)Tyr mutation in the HbI−O_2 complex and increased 10-fold by the Tyr(B10)Phe/Leu reverse mutation in the *Mt*-TrHbN−O_2 complex. In this Hb, the Gln(E11)Val/Ala single mutation decreases only ~1.5-fold the O_2 k_{on} rate and the E11 side chain may thus appear to have no role. However, the O_2 k_{on} rate is remarkably increased 32-fold by the Tyr(B10)Leu/ Gln(E11)Val double mutation,[55] so that there is a synergistic effect. This effect may come from a slight conformational change in the local heme environment caused by the double mutation or from a modified H_2O dynamics,[55] and not from additive steric effects. We must note that a synergistic mutational effect does not necessarily result from a synergistic role of the mutated side chains in the wild-type protein. Overall, the hydrogen bonding in the distal heme pocket is essential for O_2 binding and release but is not the only determinant of the affinity; steric barriers between the heme pocket and entrance channel are determinant as well.

These comparisons demonstrate that k_{off} is directly correlated with the geminate rate and yield but that the molecular conformation for achieving a particular k_{off} is not unique because k_{on} must also be modulated to reach the affinity for a precise function in a particular partial O_2 pressure. Although the overall conformation, the ligand pathway, the steric barriers, and the H-bond network all participate in controlling the affinity, if the organism need a k_{off} that is as low as possible, this parameter can be modulated by a single mutation.

Dynamics of NO within Ferrous HbI and HbII/III. Upon comparison of the dynamics of NO rebinding (Figure 7D), a remarkable fact is that the kinetics of the HbI–NO complex is superposed on that of the Mb–NO complex up to 25 ps but reaches that for the HbII/III–NO complex after 300 ps, whereas rebinding of NO to HbII/III is much faster at early times. At first glance, it seems that the HbI–NO complex has a behavior intermediate between those of Mb and HbII/III. The very large difference in the relative amplitude of the fast NO geminate rebinding phase, τ_{gem1} (36% for HbI vs 83% for HbII/III), indicates that NO diffuses away more easily in HbI (lower energy barrier), being retained close to the heme in HbII/III. The most probable hypothesis, in the absence of the NO-liganded Hb structure, is the interaction of Tyr(B10) and NO. However, we did not observe a six-coordinate excited species, as in the case of the HbII/III–O_2 complex. Thus, Tyr(B10) does not preclude photodissociation of NO but restricts its motion so that NO has a high probability of reacting with the heme, yielding the 83% amplitude. The time constant of the fast NO geminate rebinding phase for HbI and HbII/III (τ_{gem1} = 8 and 11 ps) almost reaches that of NO rebinding to a four-coordinate planar heme (τ = 7.5 ps; 97−98%), indicating the absence of any energy barrier.[27,56−58] Thus, HbII/III offers a mechanism for trapping NO that is different from that existing in the NO receptor guanylate cyclase[27] and in the bacterial cytochrome c'.[58] The NO geminate rebinding is monoexponential in these two NO receptors, where interaction with the proximal histidine is crucial, but it appears to be biexponential in the globin proteins,[34,44,56] because of the modulation of NO affinity by the distal heme pocket structure. In Mt-TrHbO, the two phases of NO geminate rebinding appear to be very similar to those of O_2 (5.1 ps, 75%; 18 ps, 25%; <1% NO released into solvent),[44] suggesting that NO is also held in place by hydrogen bonding and that the steric barrier is as efficient for NO as it is for O_2.

The total rebinding yield is the same for both Hbs, because the kinetics decrease to the same amplitude at 500 ps (Figure 7D), indicating the same amount of NO released in the solvent from both HbI and HbII/III (2%). This translates into similar k_{off} rates for dissociation of NO from Hbs.[47] Compared to Mb, HbI and HbII/III show the same trends for NO and O_2 geminate rebinding, suggesting that the steric barrier between the heme pocket and solvent for both NO and O_2 is imposed by the same side chain(s) in both proteins. The fact that the heme group seems to be less accessible in HbII/III than in HbI, as seen from the X-ray structures,[38,39] results in a lower k_{on} in HbII/III than in HbI (Table 3), not only for NO but also for O_2, as illustrated by the "sliding scale rule" for O_2 and NO binding.[59]

CONCLUSIONS

We have shown in this work that photodissociation of H_2S occurs for both ferrous and ferric HbI liganded with H_2S and is followed by very fast H_2S geminate rebinding in the ferric form with a time constant τ_{gem} of 12 ± 1 ps and a large amplitude (76%), whereas it is much slower in the ferrous form (165 ps) with a large release of H_2S into the solvent (80%). We have also shown that H_2S geminate rebinding and escape can be modulated by the hydrogen bonding network with distal side chains. In recent years, the therapeutic potentials of H_2S have been recognized, and the need for donors that can release H_2S in a controllable manner is growing. The fact that H_2S photodissociates and the fact that its release can be controlled

by the heme environment and oxidation state make cognate heme proteins potential candidates for H_2S donors.

Despite having the same tertiary structures, ferrous HbI and HbII/III show very different reactivities toward the diatomic heme ligands O_2 and NO. Whereas rebinding of O_2 to HbI is similar to that of myoglobin, it appears to be faster to HbII/III, with a larger yield. Remarkably, for both HbI and HbII/III, the rebinding of NO follows the same trend as that of O_2, showing that a HbII/III possesses a structural feature, most probably Tyr(B10), which traps both NO and O_2 close to the heme. In contrast with HbI and Mb, in HbII/III the side chains of Gln(E7) and Tyr(B10) hold O_2 in place and induce a considerable decrease in the rate of escape of O_2 into the heme pocket and solvent. In $Lucina$ HbII/III, the hydrogen bonds between Tyr(B10) and Gln(E7) and bound O_2 increase the proportion of the vibrationally photoexcited six-coordinate Fe−O_2 complex.

As seen for Hbs from $L.$ $pectinata$, several truncated hemoglobins may coexist in the same organism,[60] having diverse kinetic properties and affinity for O_2 and NO, and should correspond to different functions in the cell. The function of Hb from a protozoan[61] appears to be more complex than a carrier, and DHP, a peroxidase with a globin fold that binds H_2S, appears to have multiple functions.[62] The hydrogen bonding network, involving distal Tyr(B10), is essential for O_2 release but is not the only determinant of O_2 binding; steric barriers in the entrance channel are also determinant. Resonance Raman data showed that the Fe−His vibrational mode in HbII falls into the group of heme proteins responsible for O_2 transport.[38] Considering the very different behaviors for O_2 trapping among HbII/III, HbI, and Mb revealed by their respective geminate rebindings, it appears that HbII/III may have a more complex function, which should be investigated further.

ASSOCIATED CONTENT

S **Supporting Information**

Figures S1−S6, Scheme S1, and Tables S1−S4. This material is available free of charge via the Internet at http://pubs.acs.org.

AUTHOR INFORMATION

Corresponding Author

*E-mail: michel.negrerie@polytechnique.fr. Telephone: (33) 133 69 50 52.

Present Address

§B.-K.Y.: Physical Biology Center for Ultrafast Science and Technology, Arthur Amos Noyes Laboratory of Chemical Physics, California Institute of Technology, Pasadena, CA 91125.

Author Contributions

C.R.-A. and B.-K.Y. contributed equally to this work.

Notes

The authors declare no competing financial interest.

■ ABBREVIATIONS

HbI and HbII/III, *L. pectinata* hemoglobin types I and II/III, respectively; *Mt*-TrHb(O), truncated hemoglobin (type O or N) from *M. tuberculosis*; Mb, myoglobin; Cyt *c*, mitochondrial cytochrome *c*; TA, transient absorption; SVD, singular-value decomposition; DAS, decay-associated spectra; WT, wild type; 5-c, five-coordinate.

■ REFERENCES

(1) Frenkiel, L., Gros, O., and Moueza, M. (1996) Gill structure in *Lucina pectinata* (Bivalvia: Lucinidae) with reference to hemoglobin in bivalves with symbiotic sulphur-oxidizing bacteria. *Mar. Biol. (Heidelberg, Ger.) 125*, 511–524.

(2) Kraus, D. W., and Wittenberg, J. B. (1990) Hemoglobins of the *Lucina pectinata*/bacteria symbiosis: Molecular properties, kinetics and equilibria of reactions with ligands. *J. Biol. Chem. 265*, 16043–16053.

(3) Kendrew, J. C. (1963) Myoglobin and structure of proteins: Crystallographic analysis and data processing techniques reveal molecular architecture. *Science 139*, 1259–1266.

(4) Huang, X., and Boxer, S. G. (1994) Discovery of new ligand binding pathways in myoglobin by random mutagenesis. *Nat. Struct. Biol. 1*, 226–229.

(5) Sugimoto, T., Unno, M., Shiro, Y., Dou, Y., and Ikeda-Saito, M. (1998) Myoglobin mutants giving the largest geminate yield in CO rebinding in the nanosecond time domain. *Biophys. J. 75*, 2188–2194.

(6) Eich, R. F., Li, T., Lemon, D. D., Doherty, D. H., Curry, S. R., Aitken, J. F., Mathews, A. J., Johnson, K. A., Smith, R. D., Phillips, G. N., and Olson, J. S. (1996) Mechanism of NO-induced oxidation of myoglobin and hemoglobin. *Biochemistry 35*, 6976–6983.

(7) Kholodenko, Y., Gooding, E. A., Dou, Y., Ikeda-Saito, M., and Hochstrasser, R. M. (1999) Heme protein dynamics revealed by geminate nitric oxide recombination in mutants of iron and cobalt myoglobin. *Biochemistry 38*, 5918–5924.

(8) Pietri, R., León, R. G., Kiger, L., Marden, M. C., Granell, L. B., Cadilla, C. L., and López-Garriga, J. (2006) Hemoglobin I from *Lucina pectinata*: A model for distal heme-ligand control. *Biochim. Biophys. Acta 1764*, 758–765.

(9) Salter, M. D., Nienhaus, K., Nienhaus, G. U., Dewilde, S., Moens, L., Pesce, A., Nardini, M., Bolognesi, M., and Olson, J. S. (2008) The apolar channel in *Cerebratulus lacteus* hemoglobin is the route for O$_2$ entry and exit. *J. Biol. Chem. 283*, 35689–35702.

(10) Pietri, R., Lewis, A., Leon, R. G., Casabona, G., Kiger, L., Yeh, S., Fernandez-Alberti, S., Marden, M. C., Cadilla, C. L., and Lopez-Garriga, J. (2009) Factor controlling the reactivity of hydrogen sulfide with hemeproteins. *Biochemistry 48*, 4881–4894.

(11) Abe, K., and Kimura, H. (1996) The possible role of hydrogen sulfide as an endogenous neuromodulator. *J. Neurosci. 76*, 1066–1071.

(12) Varaksin, A. A., and Puschina, E. V. (2011) Hydrogen sulfide as a regulator of systemic functions in vertebrates. *Neurophysiology 43*, 62–72.

(13) Mustafa, A. K., Gadalla, M. M., and Snyder, S. H. (2009) Signaling by gasotransmitters. *Sci. Signaling 2*, 1–8.

(14) Szabo, C. (2007) Hydrogen sulphide and its therapeutic potential. *Nat. Rev. Drug Discovery 6*, 917–935.

(15) Brittain, T., Yosaatmadja, Y., and Henty, K. (2008) The interaction of human neuroglobin with hydrogen sulphide. *IUBMB Life 60*, 135–138.

(16) Cooper, C. E., and Brown, G. C. (2008) The inhibition of mitochondrial cytochrome oxidase by the gases carbon monoxide, nitric oxide, hydrogen cyanide and hydrogen sulfide: Chemical mechanism and physiological significance. *J. Bioenerg. Biomembr. 40*, 533–539.

(17) Koutmos, M., Kabil, O., Smith, J. L., and Banerjee, R. (2010) Structural basis for substrate activation and regulation by cystathionine β-synthase (CBS) domains in cystathionine β-synthase. *Proc. Natl. Acad. Sci. U.S.A. 107*, 20958–20963.

(18) Weeks, C. L., Singh, S., Madzelan, P., Banerjee, R., and Spiro, T. G. (2009) Heme regulation of human cystathionine-synthase activity: Insights from fluorescence and Raman spectroscopy. *J. Am. Chem. Soc. 131*, 12809–12816.

(19) Hosoki, R., Matsuki, N., and Kimura, H. (1997) The possible role of hydrogen sulfide as an endogenous smooth muscle relaxant in synergy with nitric oxide. *Biochem. Biophys. Res. Commun. 237*, 527–531.

(20) Pong, W. W., and Eldred, W. D. (2009) Interactions of the gaseous neuromodulators nitric oxide, carbon monoxide, and hydrogen sulfide in the salamander retina. *J. Neurosci. Res. 87*, 2356–2364.

(21) Yamamoto, T., Takano, N., Ishiwata, K., and Suematsu, M. (2011) Carbon monoxide stimulates global protein methylation via its inhibitory action on cystathionine β-synthase. *J. Clin. Biochem. Nutr. 48*, 96–100.

(22) Coletta, C., Papapetropoulos, A., Erdelyi, K., Olah, G., Módis, K., Panopoulos, P., Asimakopoulou, A., Gerö, D., Sharina, I., Martin, E., and Szabo, C. (2012) Hydrogen sulfide and nitric oxide are mutually dependent in the regulation of angiogenesis and endothelium-dependent vasorelaxation. *Proc. Natl. Acad. Sci. U.S.A. 109*, 9161–9166.

(23) Ramos, C., Pietri, R., Lorenzo, W., Roman, E., Cadilla, C., and Lopez-Garriga, J. (2010) Recombinant hemoglobin II from *Lucina Pectinata*: A large scale method for hemeprotein expression in *E. coli*. *Protein J. 29*, 143–151.

(24) León, R. G., Munier-Lehmann, H., Barzu, O., Baudin-Creuza, V., Pietri, R., López-Garriga, J., and Cadilla, C. L. (2004) High-level production of recombinant sulfide-reactive hemoglobin I from *Lucina pectinata* in *Escherichia coli*. *Protein Expression Purif. 38*, 184–195.

(25) Negrerie, M., Cianetti, S., Vos, M. H., Martin, J.-L., and Kruglik, S. G. (2006) Photoinduced coordination dynamics of cytochrome *c*: Ferrous versus ferric species studied by time-resolved resonance Raman and transient absorption spectroscopies. *J. Phys. Chem. B 110*, 12766–12781.

(26) Ye, X., Demidov, A., Rosca, F., Wang, W., Kumar, A., Ionascu, D., Zhu, L. Y., Barrick, D., Wharton, D., and Champion, P. M. (2003) Investigations of heme protein absorption line shapes, vibrational relaxation, and resonance Raman scattering on ultrafast time scales. *J. Phys. Chem. A 107*, 8156–8165.

(27) Yoo, B.-K., Lamarre, I., Martin, J.-L., and Negrerie, M. (2012) Quaternary structure controls ligand dynamics in soluble guanylate cyclase. *J. Biol. Chem. 287*, 6851–6859.

(28) Petrich, J. W., Poyart, C., and Martin, J. L. (1988) Photophysics and reactivity of heme-proteins: A femtosecond absorption study of hemoglobin, myoglobin and protoheme. *Biochemistry 27*, 4049–405.

(29) Cao, W., Christian, J. F., Champion, P. M., Rosca, F., and Sage, J. T. (2001) Water penetration and binding to ferric myoglobin. *Biochemistry 40*, 5728–5737.

(30) Ikeda-Saito, M., Hori, H., Andersson, L. A., Prince, R. C., Pickering, I. J., George, G. N., Sanders, C. R., Lutz, R. S., McKelvey, E. J., and Mattera, R. (1992) Coordination structure of the ferric heme iron in engineered distal histidine myoglobin mutants. *J. Biol. Chem. 267*, 22843–22852.

(31) Stone, J. R., Sands, R. H., Dunham, W. R., and Marletta, M. A. (1996) Spectral and ligand-binding properties of an unusual hemoprotein, the ferric form of soluble guanylate cyclase. *Biochemistry 35*, 3258–3262.

(32) Goldbeck, R. A., Bhaskaran, S., Ortega, C., Mendoza, J. L., Olson, J. S., Soman, J., Kliger, D. S., and Esquerra, R. M. (2006) Water and ligand entry in myoglobin: Assessing the speed and extent of heme pocket hydration after CO photodissociation. *Proc. Natl. Acad. Sci. U.S.A. 103*, 1254–1259.

(33) Peterson, E. S., Huang, S. C., Wang, J. Q., Miller, L. M., Vidugiris, G., Kloek, A. P., Goldberg, D. E., Chance, M. R., Wittenberg, J. B., and Friedman, J. M. (1997) A comparison of functional and structural consequences of the tyrosine B10 and glutamine E7 motifs in two invertebrate hemoglobins (*Ascaris suum* and *Lucina pectinata*). *Biochemistry 36*, 13110–13121.

(34) Kruglik, S. G., Yoo, B.-K., Franzen, S., Vos, M. H., Martin, J.-L., and Negrerie, M. (2010) Picosecond primary structural transition of

the heme is retarded after nitric oxide binding to heme proteins. *Proc. Natl. Acad. Sci. U.S.A. 107*, 13678−13783.

(35) Ionascu, D., Gruia, F., Ye, X., Yu, A. C., Rosca, F., Beck, C., Demidov, A., Olson, J. S., and Champion, P. M. (2005) Temperature-dependent studies of NO recombination to heme and heme proteins. *J. Am. Chem. Soc. 127*, 16921−16934.

(36) Helbing, J., Bonacina, L., Pietri, R., Bredenbeck, J., Hamm, P., van Mourik, F., Chaussard, F., Gonzalez-Gonzalez, A., Chergui, M., Ramos-Alvarez, C., Ruiz, C., and López-Garriga, J. (2004) Time-resolved visible and infrared study of the cyano complexes of myoglobin and of hemoglobin I from *Lucina pectinata*. *Biophys. J. 87*, 1881−1891.

(37) Gautier, C., Negrerie, M., Wang, Z.-Q., Lambry, J.-C., Stuehr, D. J., Collin, F., Martin, J.-L., and Slama-Schwok, A. (2004) Dynamic regulation of the inducible nitric-oxide synthase by NO: Comparaison with the endothelial isoform. *J. Biol. Chem. 279*, 4358−4365.

(38) Gavira, J. A., Camara-Artigas, A., De Jesus-Bonilla, W., Lopez-Garriga, J., Lewis, A., Pietri, R., Yeh, S.-R., Cadilla, C. L., and Garcia-Ruiz, J. M. (2008) Structure and ligand selection of hemoglobin II from *Lucina pectinata*. *J. Biol. Chem. 283*, 9414−9423.

(39) Rizzi, M., Wittenberg, J. B., Coda, A., Fasano, M., Ascenzi, P., and Bolognesi, M. (1994) Structure of the sulfide-reactive hemoglobin from the clam *Lucina pectinata*: Crystallographic analysis at 1.5 Å resolution. *J. Mol. Biol. 244*, 86−99.

(40) Rizzi, M., Wittenberg, J. B., Coda, A., Ascenzi, P., and Bolognesi, M. (1996) Structural bases for sulfide recognition in *Lucina pectinata* hemoglobin I. *J. Mol. Biol. 258*, 1−5.

(41) Ramos-Santana, B. J., and Lopez-Garriga, J. (2012) Tyrosine B10 triggers a heme propionate hydrogen bonding network loop with glutamine E7 moiety. *Biochem. Biophys. Res. Commun. 424*, 771−776.

(42) Liebl, U., Bouzhir-Sima, L., Negrerie, M., Martin, J.-L., and Vos, M. H. (2002) Ultrafast ligand rebinding in the heme domain of the oxygen sensors FixL and Dos: General regulatory implications for heme-based sensors. *Proc. Natl. Acad. Sci. U.S.A. 99*, 12771−12776.

(43) Kruglik, S. G., Jasaitis, A., Hola, K., Yamashita, T., Liebl, U., Martin, J.-L., and Vos, M. H. (2007) Subpicosecond oxygen trapping in the heme pocket of the oxygen sensor FixL observed by time-resolved resonance Raman spectroscopy. *Proc. Natl. Acad. Sci. U.S.A. 104*, 7408−7413.

(44) Jasaitis, A., Ouellet, H., Lambry, J. C., Martin, J. L., Friedman, J. M., Guertin, M., and Vos, M. H. (2012) Ultrafast heme-ligand recombination in truncated hemoglobin HbO from *Mycobacterium tuberculosis*: A ligand cage. *Chem. Phys. 396*, 10−16.

(45) Petrich, J. W., Lambry, J. C., Balasubramanian, S., Lambright, D. G., Boxer, S. G., and Martin, J. L. (1994) Ultrafast measurements of geminate recombination of NO with site-specific mutants of human myoglobin. *J. Mol. Biol. 238*, 437−444.

(46) Collazo, E., Pietri, R., De Jesús, W., Ramos, C., Del Toro, A., León, R. G., Cadilla, C. L., and López-Garriga, J. (2004) Functional characterization of the purified holo form of hemoglobin I from *Lucina pectinata* overexpressed in *Escherichia coli*. *Protein J. 23*, 239−245.

(47) De Jesus-Bonilla, W., Jia, Y. P., Alayash, A. I., and Lopez-Garriga, J. (2007) The heme pocket geometry of *Lucina pectinata* hemoglobin II restricts nitric oxide and peroxide entry: Model of ligand control for the design of a stable oxygen carrier. *Biochemistry 46*, 10451−10460.

(48) Birukou, I., Schweers, R. L., and Olson, J. S. (2010) Distal histidine stabilizes bound O_2 and acts as a gate for ligand entry in both subunits of adult human hemoglobin. *J. Biol. Chem. 285*, 8840−8854.

(49) Gibson, Q. H., Regan, R., Olson, J. S., Carver, T. E., Dixon, B., Pohajdak, B., Sharma, P. K., and Vinogradov, S. N. (1993) Kinetics of ligand binding to *Pseudoterranova decipiens* and *Ascaris suum* hemoglobins and to Leu-29 to Tyr sperm whale myoglobin mutant. *J. Biol. Chem. 268*, 16993−16998.

(50) Carver, T. E., Brantley, R. E., Singleton, E. W., Arduini, R. M., Quillin, M. L., Phillips, G. N., and Olson, J. S. (1992) A novel site-directed mutant of myoglobin with an unusually high O_2 affinity and low autooxidation rate. *J. Biol. Chem. 267*, 14443−14450.

(51) Draghi, F., Miele, A. E., Travaglini-Allocatelli, C., Vallone, B., Brunori, M., Gibson, Q. H., and Olson, J. S. (2002) Controlling ligand binding in myoglobin by mutagenesis. *J. Biol. Chem. 277*, 7509−7519.

(52) Manon, C., Das, T. K., Lee, H. C., Peisach, J., Rousseau, D., Wittenberg, B. A., Wittenberg, J. B., and Guertin, M. (1999) *Chlamydomonas* chloroplast ferrous hemoglobin: Heme pocket structure and reactions with ligands. *J. Biol. Chem. 274*, 6898−6910.

(53) Golberg, D. E. (1999) Oxygen-avid hemoglobin of *Ascaris*. *Chem. Rev. 99*, 3371−3378.

(54) Ouellet, H., Juszczak, L., Dantsker, D., Samuni, U., Ouellet, Y. H., Savard, P.-Y., Wittenberg, J. B., Wittenberg, B. A., Friedman, J. M., and Guertin, M. (2003) Reactions of *Mycobacterium tuberculosis* truncated hemoglobin O with ligands reveal a novel ligand-inclusive hydrogen bond network. *Biochemistry 42*, 5764−5774.

(55) Ouellet, Y. H., Daigle, R., Lagüe, P., Dantsker, D., Milani, M., Bolognesi, M., Friedman, J. M., and Guertin, M. (2008) Ligand binding to truncated hemoglobin N from *Mycobacterium tuberculosis* is strongly modulated by the interplay between the distal heme pocket residues and internal water. *J. Biol. Chem. 283*, 27270−27278.

(56) Negrerie, M., Kruglik, S. G., Lambry, J.-C., Vos, M. H., Martin, J.-L., and Franzen, S. (2006) Role of heme iron coordination and protein structure in the dynamics and geminate rebinding of nitric oxide to H93G myoglobin: Implications for NO-sensors. *J. Biol. Chem. 281*, 10389−10398.

(57) Kruglik, S. G., Lambry, J.-C., Cianetti, S., Martin, J.-L., Eady, R. R., Andrew, C. R., and Negrerie, M. (2007) Molecular basis for nitric oxide dynamics and affinity with *Alcaligenes xylosoxidans* cytochrome c′. *J. Biol. Chem. 282*, 5053−5062.

(58) Yoo, B.-K., Lamarre, I., Martin, J.-L., Andrew, C., and Negrerie, M. (2013) Picosecond binding of the His ligand to four-coordinate heme in cytochrome c′: A one-way gate for releasing proximal NO. *J. Am. Chem. Soc. 135*, 3248−3254.

(59) Tsai, A.-L., Berka, V., Martin, E., and Olson, J. S. (2012) A "sliding scale rule" for selectivity among NO, CO, and O_2 by heme protein sensors. *Biochemistry 51*, 172−186.

(60) Lu, C., Egawa, T., Mukai, M., Poole, R. K., and Yeh, S.-R. (2008) Hemoglobins from *Mycobacterium tuberculosis* and *Campylobacter jejuni*: A comparative study with resonance Raman spectroscopy. *Methods Enzymol. 437*, 255−286.

(61) Igarashi, J., Kobayashi, K., and Matsuoka, A. (2011) A hydrogen-bonding network formed by the B10-E7-E11 residues of a truncated hemoglobin from *Tetrahymena pyriformis* is critical for stability of bound oxygen and nitric oxide detoxification. *JBIC, J. Biol. Inorg. Chem. 16*, 599−609.

(62) Nicoletti, F. P., Thompson, M. K., Franzen, S., and Smulevich, G. (2011) Degradation of sulfide by dehaloperoxidase-hemoglobin from *Amphitrite ornata*. *JBIC, J. Biol. Inorg. Chem. 16*, 611−619.

(63) Wan, L., Twitchett, M. B., Eltis, L. D., Mauk, A. G., and Smith, M. (1998) In vitro evolution of horse heart myoglobin to increase peroxidase activity. *Proc. Natl. Acad. Sci. U.S.A. 95*, 12825−12831.

(64) Kharitonov, V. G., Bonaventura, J., and Sharma, V. S. (1996) In *Methods in nitric oxide research*, pp 39−45, John Wiley & Sons, New York.

(65) Brucker, E. A., Olson, J. S., Ikeda-Saito, M., and Phillips, G. N. (1998) Nitric oxide myoglobin: Crystal structure and analysis of ligand geometry. *Proteins 30*, 352−356.

(66) Dunbrack, R. L. (2002) Rotamer libraries in the 21st century. *Curr. Opin. Struct. Biol. 12*, 431−440.